

On the Steady Nature of Line-Driven Disk Winds: Application to Cataclysmic Variables

Nicolas A. Pereyra¹, David A. Turnshek, and D. John Hillier

*University of Pittsburgh, Department of Physics and Astronomy, 3941 O'Hara ST,
Pittsburgh, PA 15260*

pereyra@bruno.phyast.pitt.edu, turnshek@quasar.phyast.pitt.edu,
jdh@galah.phyast.pitt.edu

ABSTRACT

We apply the semi-analytical analysis of the steady nature of line-driven winds presented in two earlier papers to disk winds driven by the flux distribution of a standard Shakura & Sunyaev (1973) disk for typical cataclysmic variable (CV) parameters. We find that the wind critical point tends to be closer to the disk surface towards the inner disk regions. Our main conclusion, however, is that a line-driven wind, arising from a steady disk flux distribution of a standard Shakura-Sunyaev disk capable of locally supplying the corresponding mass flow, is steady. These results confirm the findings of an earlier paper that studied “simple” flux distributions that are more readily analyzable than those presented here. These results are consistent with the steady velocity nature of outflows observationally inferred for both CVs and quasi-stellar objects (QSOs). We find good agreement with the 2.5D CV disk wind models of Pereyra and collaborators. These results suggest that the likely scenario to account for the wind outflows commonly observed in CVs is the line-driven accretion disk wind scenario, as suggested early-on by Córdova & Mason (1982). For QSOs, these results show that the line-driven accretion disk wind continues to be a promising scenario to account for the outflows detected in broad absorption line (BAL) QSOs, as suggested early-on by Turnshek (1984), and analyzed in detail by Murray et al. (1995).

Subject headings: accretion, accretion disks — hydrodynamics — novae, cataclysmic variables — QSOs: absorption lines

¹Also at: Universidad Marítima del Caribe, Departamento de Ciencias Básicas, Catia la Mar, Venezuela

1. Introduction

As discussed in Pereyra et al. (2004, hereafter Paper I) and Pereyra (2005, hereafter Paper II), accretion disks are commonly believed to be present in both cataclysmic variables (CVs) and quasi-stellar objects and active galactic nuclei (QSOs/AGNs). A property that CVs and QSOs have in common is that both types of objects sometimes present blue-shifted absorption troughs in UV resonance lines, giving direct observational evidence for an out-flowing wind. Both types of objects also show the existence of a persistent velocity structure in their absorption troughs (when present) over significantly long time scales (Paper I).

In order for a disk wind to account for the wide/broad resonance line absorption structures observed in many CVs and QSOs, it must be able to account for the steady velocity structure that is observed. The 2.5D time-dependent disk wind models of Pereyra and collaborators, both for CVs and QSOs, have steady disk wind solutions (Pereyra 1997; Pereyra, Kallman, & Blondin 1997, 2000; Hillier et al. 2002; Pereyra & Kallman 2003). The earlier 1D disk wind models of Murray and collaborators also find steady disk wind solutions (Murray et al. 1995; Murray & Chiang 1996; Chiang & Murray 1996; Murray & Chiang 1998).

However, in the literature it has been argued that line-driven disk winds are “intrinsically unsteady” because of the increasing gravity along the streamlines at wind base that is characteristic of disk winds (see Paper I; Paper II). Since the steady nature of CV and QSO wind flows is an observational constraint, whether line-driven disk winds are steady is a significant issue. Our objective is to study this issue through a semi-analytical method independent of our previous 2.5D numerically intensive simulation efforts (e.g., Pereyra 1997; Pereyra, Kallman, & Blondin 2000).

In Paper I we showed that an increase in gravity at wind base, that is characteristic of disk winds, does *not* imply an unsteady wind solution. We also developed mathematically “simple” models that mimic the disk environment and we showed that *line-driven disk winds can be steady*. In Paper II we extended the concepts presented in Paper I, and discussed in detail many aspects that were mentioned in Paper I.

The goal of this paper is to apply the concepts introduced in Paper I and Paper II to more realistic models that implement the exact flux distribution above a standard accretion disk. We compare and find good agreement with the steady CV disk wind solutions found through numerically intensive calculations by Pereyra (1997) and Pereyra, Kallman, & Blondin (2000).

In §2 we present a general discussion of the reduction of the 2.5D models of Pereyra (1997); Pereyra, Kallman, & Blondin (2000) to a series of 1D models by neglecting radial

terms. We shall see that, although this a rough approximation high above the disk, it is quite accurate near the disk surface. We reduce the 2.5D model of Pereyra and collaborators to a series of 1D equations in §3. In §4 we present the results of our series of 1D models for different disk radius. We show that the critical point in the inner disk regions is found near the disk surface, allowing for an analysis of the solutions with steady wind mass loss rates. A summary and conclusions are presented in §5.

2. General Comments

The analysis of existence for steady line-driven wind solutions discussed in Paper I and Paper II correspond to 1D models. Thus, to apply them to a 2.5D model, we first reduce the 2.5D model to a series of 1D models. To do this we consider the following: the wind in CVs tend to be vertical (perpendicular to the disk). There is observational, theoretical, and computational evidence for this. In CVs the P-Cygni type line profiles are observed only in low inclination systems (close to disk face-on) and with high inferred disk mass accretion rates (e.g., Warner 1995). This orientation angle effect was one of the observational properties of CVs that led to the early suggestion by Córdova & Mason (1982) that the outflows detected in CVs originate from the accretion disk.

From a theoretical standpoint, if the wind originates from a steady disk, then the radial forces at wind base (disk surface) must be at equilibrium, thus the wind must start off vertical. We note here that by “vertical” we actually mean “non-radial,” since the wind starts off with an azimuthal component due to disk rotation. We also note here that although the disk wind must in principal start vertical at its base, this does not necessarily imply that the wind will continue predominantly vertical. For example, in the case of QSOs/AGNs, disk wind models (Murray et al. 1995; Hillier et al. 2002) indicate that the wind tends to quickly become radial in nature.

However, computational 2.5D models of CV disk winds have produced winds that tend to be vertical in nature. Theoretical resonance line profiles calculated from these models are consistent with observed line profiles in their general form, in the magnitudes of wind velocities implied by the absorption components, in the FWHM of the emission components, and in the strong dependence with inclination angle (Pereyra 1997; Pereyra, Kallman, & Blondin 2000).

Therefore, near the wind base (disk surface), a CV disk wind at a given radius can be well approximated by a vertical 1D model. High above the disk rotational forces come into play (no longer at equilibrium with the radial component of gravity), streamlines collide,

and the density/velocity wind structure will be 2.5D (i.e., 2D with an azimuthal velocity component) (Pereyra 1997; Pereyra, Kallman, & Blondin 1997, 2000; Pereyra & Kallman 2003). Although a 1D vertical model is not accurate high above the disk for the above reasons, it does give accurate results near wind base.

As was shown by Castor, Abbott, & Klein (1975) for early type stars, and was discussed in Paper II for 1D line-driven winds, the wind mass loss rate is determined by the position of the critical point. As we show below, for the CV parameters we use in this section [taken from the models of Pereyra, Kallman, & Blondin (2000)], at radii where there is significant contributions to the wind mass loss, the critical point is near the disk surface. Therefore, disk wind characteristics for 2.5D CV models can be addressed.

3. Reduction to a Series of 1D Models

The equations of state, mass, and momentum of the 2.5D CV disk wind model of Pereyra, Kallman, & Blondin (2000) are, respectively:

$$P = \rho b^2 \quad ; \quad (1)$$

$$\frac{\partial \rho}{\partial t} + \frac{1}{r} \frac{\partial(r\rho V_r)}{\partial r} + \frac{\partial(\rho V_z)}{\partial z} = 0 \quad ; \quad (2)$$

and

$$\begin{aligned} \rho \frac{\partial V_r}{\partial t} + \rho V_r \frac{\partial V_r}{\partial r} - \rho \frac{V_\phi^2}{r} + \rho V_z \frac{\partial V_r}{\partial z} &= -\rho \frac{GM_{wd}}{(r^2 + z^2)} \frac{r}{(r^2 + z^2)^{1/2}} - \frac{\partial P}{\partial r} + \rho \frac{\kappa_e \mathcal{F}_r(r, z)}{c} \\ &+ \rho \frac{\kappa_e S_r(r, z)}{c} \times k \left(\max \left[\frac{1}{\rho \kappa_e V_{th}} \left| \frac{\partial V_z}{\partial z} \right|, 10^8 \right] \right)^\alpha ; \end{aligned} \quad (3)$$

$$\rho \frac{\partial V_\phi}{\partial t} + \rho V_r \frac{\partial V_\phi}{\partial r} + \rho \frac{V_\phi V_r}{r} + \rho V_z \frac{\partial V_\phi}{\partial z} = 0 \quad ; \quad (4)$$

$$\begin{aligned} \rho \frac{\partial V_z}{\partial t} + \rho V_r \frac{\partial V_z}{\partial r} + \rho V_z \frac{\partial V_z}{\partial z} &= -\rho \frac{GM_{wd}}{(r^2 + z^2)} \frac{z}{(r^2 + z^2)^{1/2}} - \frac{\partial P}{\partial z} + \rho \frac{\kappa_e \mathcal{F}_z(r, z)}{c} \\ &+ \rho \frac{\kappa_e S_z(r, z)}{c} \times k \left(\max \left[\frac{1}{\rho \kappa_e V_{th}} \left| \frac{\partial V_z}{\partial z} \right|, 10^8 \right] \right)^\alpha ; \end{aligned} \quad (5)$$

where P is the pressure, ρ is the density, b is the isothermal sound speed, V_r , V_ϕ , and V_z are the corresponding velocity components in cylindrical coordinates, G is the gravitational constant, M_{wd} is the mass of the white dwarf, κ_e is the Thomson cross section per mass, c is the speed of light, V_{th} is the ion thermal velocity, and k and α are the CAK line force parameters. \mathcal{F}_z and \mathcal{F}_r are the corresponding radiation flux components given by:

$$\mathcal{F}_z(r, z) = \int_{r_i}^{\infty} \int_0^{2\pi} \frac{Q(r')}{\pi} \frac{z^2}{\left[(r^2 + r'^2 + z^2 - 2rr' \cos \phi)^{1/2} \right]^4} r' d\phi dr' \quad , \quad (6)$$

and

$$\mathcal{F}_r(r, z) = \int_{r_i}^{\infty} \int_0^{2\pi} \frac{Q(r')}{\pi} \frac{z(r - r' \cos \phi)}{\left[(r^2 + r'^2 + z^2 - 2rr' \cos \phi)^{1/2} \right]^4} r' d\phi dr' \quad , \quad (7)$$

S_z and S_r are defined as:

$$S_z(r, z) \equiv \int_{r_i}^{\infty} \int_0^{2\pi} \frac{Q(r')}{\pi} \frac{z^{\alpha+2}}{\left[(r^2 + r'^2 + z^2 - 2rr' \cos \phi)^{1/2} \right]^{\alpha+4}} r' d\phi dr' \quad , \quad (8)$$

and

$$S_r(r, z) \equiv \int_{r_i}^{\infty} \int_0^{2\pi} \frac{Q(r')}{\pi} \frac{z^{\alpha+1}(r - r' \cos \phi)}{\left[(r^2 + r'^2 + z^2 - 2rr' \cos \phi)^{1/2}\right]^{\alpha+4}} r' d\phi dr' \quad , \quad (9)$$

where in turn $Q(r)$ is the rate of energy per area, at a given radius r , radiated by a standard disk (Shakura & Sunyaev 1973), that is:

$$Q(r) = \frac{3\dot{M}_{accr}GM_{wd}}{8\pi r^3} \left[1 - \left(\frac{r_i}{r}\right)^{1/2}\right] \quad , \quad (10)$$

where r_i is the inner disk radius. In CVs, r_i is approximately equal to the white dwarf radius. We note that in equations (6)-(9) there is an implicit assumption that $r_i \ll r_f$, where r_f is the outer disk radius.

The total disk luminosity \mathcal{L}_{disk} is given by

$$\mathcal{L}_{disk} = \int_{r_i}^{r_f} 4\pi r Q(r) dr \quad , \quad (11)$$

where r_f is the outer disk radius. Thus

$$\mathcal{L}_{disk} = \frac{\dot{M}_{accr}GM_{wd}}{2r_i} \left\{1 - \frac{3r_i}{r_f} \left[1 - \frac{2}{3} \left(\frac{r_i}{r_f}\right)^{1/2}\right]\right\} \quad ; \quad (12)$$

assuming $r_i \ll r_f$

$$\mathcal{L}_{disk} \approx \frac{\dot{M}_{accr}GM_{wd}}{2r_i} \quad . \quad (13)$$

We define

$$\Gamma \equiv \frac{\kappa_e \mathcal{L}_{disk}}{4\pi GM_{wd} c} \quad . \quad (14)$$

Considering equations (13) and (14), equation (10) can be rewritten as

$$Q(r) = 3 \frac{c}{\kappa_e} \frac{GM_{wd}}{r_i^2} \Gamma \left(\frac{r_i}{r}\right)^3 \left[1 - \left(\frac{r_i}{r}\right)^{1/2}\right] \quad . \quad (15)$$

Additionally, we define two dimensionless functions $\Upsilon(r, z)$ and $\zeta(r, z)$:

$$\Upsilon(r, z) \equiv \int_{r_i}^{\infty} \int_0^{2\pi} \frac{1}{\pi} \left(\frac{r_i}{r'}\right)^3 \left[1 - \left(\frac{r_i}{r'}\right)^{1/2}\right] \frac{z^2}{\left[(r^2 + r'^2 + z^2 - 2rr' \cos \phi)^{1/2}\right]^4} r' d\phi dr' \quad ; \quad (16)$$

$$\zeta(r, z) \equiv \int_{r_i}^{\infty} \int_0^{2\pi} \frac{1}{\pi} \left(\frac{r_i}{r'}\right)^3 \left[1 - \left(\frac{r_i}{r'}\right)^{1/2}\right] \frac{z^{\alpha+2}}{\left[(r^2 + r'^2 + z^2 - 2rr' \cos \phi)^{1/2}\right]^{\alpha+4}} r' d\phi dr' \quad . \quad (17)$$

It follows that

$$\mathcal{F}_z(r, z) = 3 \frac{c}{\kappa_e} \frac{GM_{wd}}{r_i^2} \Gamma \Upsilon(r, z) = 3 \frac{\mathcal{L}_{disk}}{4\pi r_i^2} \Upsilon(r, z) \quad ; \quad (18)$$

$$S_z(r, z) = 3 \frac{c}{\kappa_e} \frac{GM_{wd}}{r_i^2} \Gamma \zeta(r, z) = 3 \frac{\mathcal{L}_{disk}}{4\pi r_i^2} \zeta(r, z) \quad . \quad (19)$$

In reducing the 2.5D model to a series of 1D models, for simplicity, we assume an isothermal wind. We do not expect this approximation to significantly change the results of this work, as is illustrated in the intermediate models of Pereyra, Kallman, & Blondin (2000) [see Figures 6 and 7 of Pereyra, Kallman, & Blondin (2000)]. This, on one hand, significantly simplifies the analysis, and on the other hand gives a predefined temperature structure [namely: $b^2(x) = \text{constant}$] that is a requirement of the 1D models of this work (see Paper I; Paper II). Thus the equation of state we assume, for the application to the 2.5D CV disk wind model, is

$$\frac{P}{\rho} = b^2 \quad (\text{constant}) \quad . \quad (20)$$

We also assume that the streamlines, starting from the disk at a given radius r , are predominantly vertical. As discussed in §2, this assumption is justified on observational, theoretical, and computational grounds.

The mass conservation equation is equivalent to the 1D models of Pereyra, Kallman, & Blondin (1997), namely, for a given r

$$\dot{M} = \rho V 4\pi R^2 \quad (\text{constant}) \quad , \quad (21)$$

where we are determining the existence of 1D steady (stationary) solutions, and where

$$R^2 \equiv r^2 + z^2 \quad , \quad (22)$$

and \dot{M} is an integration constant, z is the height above the disk, and r is the radius where a given streamline begins. Thus for each value of r considered, a given 1D model is developed. We note that in equation (21), \dot{M} is not the wind mass loss rate (as in Paper I and Paper II), but only an integration constant. We have used the symbol \dot{M} following the notation of Paper I and Paper II. However, the wind mass loss rate \dot{M}_{wind} can be obtained by (after first determining the values of \dot{M} for different values of r)

$$\dot{M}_{wind} = 2 \int_{r_i}^{r_f} \frac{\dot{M}(r)}{4\pi(r^2 + z_s^2)} 2\pi r dr \quad . \quad (23)$$

For $z \ll r$, $R^2 \approx r^2$ (= constant for a given 1D model), thus for $z \ll r$, $\rho V = \text{constant}$ [equation (21)] that is the integration of equation (2) assuming stationary solutions and neglecting radial velocities. Therefore, equation (21) is accurate near the disk surface and it is also accurate towards infinity ($z \gg r$, $R^2 \approx z^2$). However, equation (21) is not accurate at intermediate values of z where 2.5D effects become important (Pereyra 1997; Pereyra, Kallman, & Blondin 1997, 2000). Using the accurate results near the disk surface, as discussed in §2, we study whether wind solutions with steady mass loss rates exist.

In reducing the 2.5D model to a series of 1D models, we additionally neglect the effect of a maximum possible value for the line radiation force (Castor, Abbott, & Klein 1975; Abbott 1982), that are represented in the models of Pereyra (1997) and Pereyra, Kallman, & Blondin (2000) by including a “max” function in the line force terms [see equation (5)]. On one hand, we do not expect this approximation to significantly change the results of this work. In the intermediate models of Pereyra, Kallman, & Blondin (2000) this effect was found to be most significant in the low density region high above the inner disk region. On the other hand, this allows the momentum equation to take a form equivalent to the momentum equation of Paper II, that is the form of the momentum equation assumed in the 1D models of this work.

Thus, within the assumption of a predominately vertical wind, assuming stationary solutions, neglecting radial velocities, and considering equation (5), the momentum equation for the 1D models (at a given r) becomes

$$\begin{aligned} \rho V \frac{dV}{dz} &= -\rho \frac{GM_{wd}}{R^2} \frac{z}{R} + \rho \frac{3GM_{wd}}{r_i^2} \Gamma \Upsilon(r, z) - \frac{dP}{dz} \\ &+ \rho \frac{3GM_{wd}}{r_i^2} \Gamma \zeta(r, z) k \left(\frac{1}{\rho \kappa_e V_{th}} \frac{\partial V}{\partial z} \right)^\alpha, \end{aligned} \quad (24)$$

where $\Upsilon(r, z)$ and $\zeta(r, z)$ are given by equations (16) and (17), respectively. The series of 1D models derived from the 2.5D disk wind model, can be represented within the 1D models of Paper II, through the following parameterization:

$$B(z) = \frac{GM_{wd}}{R^2} \frac{z}{R} - \frac{3GM_{wd}}{r_i^2} \Gamma \Upsilon(r, z) \quad , \quad (25)$$

$$A(z) = 4\pi R^2 = 4\pi (r^2 + z^2) \quad , \quad (26)$$

$$\text{and} \quad \gamma(z) = \frac{3GM_{wd}}{r_i^2} \Gamma \zeta(r, z) k \left(\frac{1}{\kappa_e V_{th}} \right)^\alpha \quad , \quad (27)$$

where the body force $B(z)$, the area function $A(z)$, and the line opacity weighted flux $\gamma(z)$ are defined for a given r . Thus, the mass conservation equation and the momentum equation have the form of the equations of Paper II. The isothermal equation of motion is therefore,

$$\left(1 - \frac{b^2}{V^2}\right) AV \frac{dV}{dz} = -BA + \gamma A \left(\frac{A}{\dot{M}} V \frac{dV}{dz}\right)^\alpha + b^2 \frac{dA}{dz} \quad . \quad (28)$$

Defining the characteristic distance r_0 , gravitational force B_0 , area A_0 , and line-opacity weighted flux γ_0 (see Paper I; Paper II) through

$$r_0 = r \quad ; \quad B_0 = \frac{GM_{wd}}{r^2} \quad ; \quad A_0 = 4\pi r^2 \quad ; \quad \gamma_0 = \frac{3GM_{wd}}{r_i^2} \Gamma k \left(\frac{1}{\kappa_e V_{th}}\right)^\alpha \quad ; \quad (29)$$

the equation of motion becomes

$$\left(1 - \frac{s}{\omega}\right) a \frac{d\omega}{dx} = -ga + fa \left(\frac{a}{\dot{m}} \frac{d\omega}{dx}\right)^\alpha + 4sx \quad , \quad (30)$$

where

$$x = \frac{z}{r} \quad ; \quad (31)$$

$$g = \frac{x}{(1+x^2)^{3/2}} - \frac{3\Gamma}{x_i^2} \Upsilon \quad ; \quad x_i \equiv \frac{r_i}{r} \quad ; \quad (32)$$

$$a = 1 + x^2 \quad ; \quad (33)$$

$$f = \frac{1}{\alpha^\alpha (1-\alpha)^{1-\alpha}} \zeta \quad . \quad (34)$$

The parameters s , ω , and \dot{m} (see Paper I; Paper II) are given by

$$s \equiv \frac{b^2}{2W_0} \quad ; \quad \omega \equiv \frac{W}{W_0} \quad ; \quad \dot{m} \equiv \frac{\dot{M}}{\dot{M}_{CAK}} \quad , \quad (35)$$

where

$$W_0 \equiv B_0 r_0 \quad ; \quad W \equiv \frac{V^2}{2} \quad ; \quad \dot{M}_{CAK} \equiv \alpha(1-\alpha)^{(1-\alpha)/\alpha} \frac{(\gamma_0 A_0)^{1/\alpha}}{(B_0 A_0)^{(1-\alpha)/\alpha}} \quad . \quad (36)$$

Taking $x_0 = 0$ and $q_0 = 0$, the spatial variable q (see Paper II)

$$q \equiv \int_{x_0}^x \frac{1}{a(x')} dx' + q_0 \quad , \quad (37)$$

becomes

$$q = \arctan(x) \quad . \quad (38)$$

The equation of motion, expressed in terms of q , becomes

$$\left(1 - \frac{s}{\omega}\right) \frac{d\omega}{dq} = h(q) + fa \left(\frac{1}{\dot{m}} \frac{d\omega}{dq}\right)^\alpha \quad , \quad (39)$$

where the function $h(q)$ is now given by

$$h(q) = -ga + 4s \tan(q) \quad . \quad (40)$$

The nozzle function n for each r is given by (Paper II):

$$n(q) \equiv \alpha(1 - \alpha)^{(1-\alpha)/\alpha} \frac{(fa)^{1/\alpha}}{(-h)^{(1-\alpha)/\alpha}} \quad \text{for} \quad h(q) < 0$$

$$\left[= \alpha(1 - \alpha)^{(1-\alpha)/\alpha} \frac{(fa)^{1/\alpha}}{(ga - 4s \tan(q))^{(1-\alpha)/\alpha}} \right] \quad . \quad (41)$$

Additionally we shall recall the definition of the β function as defined in Paper I and Paper II

$$\beta(\omega) \equiv 1 - \frac{s}{w} \quad , \quad (42)$$

that we shall apply in the following section.

Thus, we have reduced the 2.5D models to a series of 1D models by solving the hydrodynamic equations in the vertical direction and neglecting radial terms. That is, for a given radial distance r , we have a 1D model with $q = \arctan(x) = \arctan(z/r)$ as the independent spatial variable. As discussed above these models are accurate near the disk surface. Since, as we see below, the corresponding critical point for inner radii is near the disk surface, the 1D models for the inner disk regions determine that disk wind flows with steady mass loss rates are possible. The models can be used to estimate local mass loss rates (by determining local density at the sonic point) as well as velocity and density wind structure near the disk surface in the inner region.

4. Results

For the 1D wind models, we implement the set of parameters used by Pereyra, Kallman, & Blondin (2000) corresponding to a CV, namely:

$$M_{wd} = 0.6M_{\odot} \quad ; \quad \mathcal{L}_{disk} = \mathcal{L}_{\odot} \quad ; \quad z_s = 0.0229R_{\odot} \quad ;$$

$$r_i = 0.01R_{\odot} \quad ; \quad b = 10 \text{ km s}^{-1} \quad ; \quad V_{th} = 2.67 \text{ km s}^{-1} \quad . \quad (43)$$

We use the line force parameters also used by Pereyra, Kallman, & Blondin (2000) [and Castor, Abbott, & Klein (1975) and Abbott (1982)], namely

$$k = 1/3 \quad ; \quad \alpha = 0.7 . \quad (44)$$

As with the analysis of the isothermal CAK stellar wind (Paper II), we first consider, for a given r , the h function for the 1D vertical wind model with the flux distribution of a standard Shakura & Sunyaev (1973) disk. As discussed in Paper II, h must be negative at the critical point (i.e., h must be negative in order for there to exist values of q , ω , and $d\omega/dq$ that satisfy the critical point conditions). Second, we consider the nozzle function, that as we found in Paper II, for the case of an isothermal wind must be a locally increasing function at the critical point (i.e., it must have a positive spatial derivative at the critical point). Third, for the spatial points where the first two conditions hold, through the nozzle function n , the β function, the normalized wind mass loss rate \dot{m} , and the calculation of $d^2\omega/dq^2$ under critical point conditions, as discussed in Paper II, we determine if a local solution exists by verifying whether or not the condition

$$\beta''(\omega) \dot{m} (\omega')^2 + \beta'(\omega) \dot{m} \omega'' - n''(q) < 0 \quad (45)$$

holds. Fourth, within the set of points that fulfill the first three conditions, we iteratively determine the position of the critical point such that the wind reaches sound speed at the sonic height of the model (as discussed in Paper II).

As a consistency check, for a given r , we superimpose a plot of the nozzle function n and the $\beta(\omega) \dot{m}$ function evaluated with the corresponding velocities $V(z)$. As discussed in Paper II, in the supersonic wind regime where the h function is negative (Region II), for points other than the critical point, the following conditions must hold

$$\beta(\omega) \dot{m} < n(q) \quad (\text{for } \omega > s \text{ and } h(q) < 0 \text{ and } q \neq q_c) \quad , \quad (46)$$

and at the critical point

$$\beta(\omega_c) \dot{m} = n(q_c) \quad . \quad (47)$$

For $r = 2r_i$, Figure 1 shows that the h function is negative from the sonic point to beyond 1000 times the sonic height. Figure 2 shows that the nozzle function n , corresponding to a vertical streamline at $r = 2r_i$, is a monotonically increasing function from the sonic point

to beyond 1000 times the sonic height. It is shown, in Figure 3, that equation (45) holds from the sonic height to beyond 1000 times the sonic height, showing that local solutions to the equation of motion exist throughout the fore mentioned spatial region. By “local solution” at a given spatial point, we mean the integration of the equation of motion in the vicinity of the given point, assuming the point to be the critical point. Figure 4 shows the velocity vs. height obtained upon integrating the equation of motion with the condition of achieving the correct sonic height of the model. As a consistency check, Figure 5 verifies that equations (46) and (47) hold for the solution obtained.

Figures 6-10, Figures 11-15, and Figures 16-20 plot the results from an equivalent analysis to wind streamlines starting at $r = 10 r_i$, $r = 20 r_i$, and $r = 50 r_i$ respectively. The results show that steady line-driven disk wind solutions exist for a standard Shakura-Sunyaev disk.

A significant result we find is that the critical point tends to be closer to the disk surface in the inner disk regions, and farther out from the disk surface in the outer disk regions. Physically this is due to the length scales in these different regions. The disk wind, at each radii, results from the balancing of the gravitational forces and the radiation pressure forces. This balance can be presented quantitatively by the nozzle function defined in Paper I and Paper II. The spatial dependence of the nozzle function in turn is crucial in determining the critical point position. As larger disk radii are considered, the scale length of the corresponding nozzle function also increases, and therefore the critical point position increases as well.

Also, the resulting local wind mass loss rates, for the different radii considered, are in good agreement with the 2.5D numerically intensive CV disk wind models of Pereyra (1997); Pereyra, Kallman, & Blondin (2000); for example for a radius of $10r_i$ the local wind mass loss rates found in this work is $5.0 \times 10^{-7} \text{g s}^{-1} \text{cm}^{-2}$, and for the same physical model parameters the previous numerically intensive 2.5D calculations estimated a value of $7.1 \times 10^{-7} \text{g s}^{-1} \text{cm}^{-2}$ for the same radius. By confirming the overall earlier results of Pereyra and collaborators, we conclude that the likely scenario for the wind outflows in CVs is a line-driven disk wind. This scenario was suggested for CVs early on by Córdova & Mason (1982). Pereyra (1997); Pereyra, Kallman, & Blondin (2000) showed that the line-driven disk wind scenario was able to account for the general forms of the C IV $\lambda\lambda 1549$ line profile and its general dependence on viewing angle [for a review on CV properties in general, see Warner (1995)].

The steady nature of line-driven disk wind that we find here may also be relevant to QSO studies. Turnshek (1984) had suggested this scenario early-on based on observational constraints. The first serious attempt to study this scenario was by Murray et al. (1995), who developed 1D streamline models and found that this scenario could account for several QSO

observational features, such as the terminal wind velocities inferred from broad absorption lines (BALs) (when present) and the general form of single-trough BALs (when present). As discussed in the Introduction, an additional constraint on the BAL region, is that it presents a steady velocity structure. Our results here show that the line-driven disk wind scenario is consistent with the observed steady velocity structure.

Thus both observational constraints and theoretical/computational studies to date seem to indicate that the line-driven disk wind scenario is a promising one to account for the BALs commonly observed in QSOs.

In future work we plan to study several aspects of this scenario and develop more realistic models.

5. Summary and Conclusions

In Paper I we had shown that steady wind solutions can exist by using “simple” models that mimic the disk environment. These models are more readily analyzable than the more detailed models presented here. In Paper II we extended the concepts of Paper I, and discussed in detail aspects of the steady/unsteady wind analysis that was presented in Paper I. The objective of this work is to determine, in a manner independent of the results of previous numerically-intensive 2.5D hydrodynamic simulations, whether steady line-driven disk wind solutions exist under the flux distribution of a standard disk (Shakura & Sunyaev 1973).

Our main conclusion pertaining to the more realistic models presented here is that a line-driven wind, arising from a steady disk using the flux distribution of a standard Shakura-Sunyaev disk model, is steady. As we had discussed in Paper II, when including gas pressures effects, the spatial dependence of the nozzle function continues to play a key role in determining the steady/unsteady nature of supersonic line-driven wind solutions.

These results are consistent with the steady nature of the 1D streamline disk wind models of Murray and collaborators (Murray et al. 1995; Murray & Chiang 1996; Chiang & Murray 1996; Murray & Chiang 1998). These results also confirm the results of the 2.5D steady disk wind models of Pereyra and collaborators (Pereyra 1997; Pereyra, Kallman, & Blondin 2000; Hillier et al. 2002; Pereyra & Kallman 2003).

Another result that we find is that the critical point of the wind tends to be closer to the disk surface as smaller radii closer to the inner disk region are considered.

As we develop more realistic models, we aim towards placing stronger constraints on the accretion disk wind scenario, particularly as they apply to QSOs. If the scenario proves

tenable, then we may have a well-defined route towards a better understanding of these astronomically fundamental objects.

We wish to thank Kenneth G. Gayley and Norman W. Murray for many useful discussions. This work is supported by the National Science Foundation under Grant AST-0071193, and by the National Aeronautics and Space Administration under Grant ATP03-0104-0144.

REFERENCES

- Abbott, D. C. 1982, *ApJ*, 259, 282
- Castor, J. I., Abbott, D. C., & Klein, R. I. 1975, *ApJ*, 195, 157
- Chiang, J., & Murray, N. 1996, *ApJ*, 466, 704
- Córdova, F. A., & Mason, K. O. 1982, *ApJ*, 260, 716
- Hillier, D. J., Pereyra, N. A., Turnshek, D. A., & Owocki, S. P. 2002, *BAAS*, 34, 648
- Murray, N., Chiang, J., Grossman, S. A., & Voit, G. M. 1995, *ApJ*, 451, 498
- Murray, N., & Chiang, J. 1996, *Nature*, 382, 789
- Murray, N., & Chiang, J. 1998, *ApJ*, 494, 125
- Pereyra, N. A. 1997, Ph.D. Thesis, University of Maryland at College Park
- Pereyra, N. A., Kallman, T. R., & Blondin, J. M. 1997, *ApJ*, 477, 368
- Pereyra, N. A., Kallman, T. R., & Blondin, J. M. 2000, *ApJ*, 532, 563
- Pereyra, N. A., & Kallman, T. R. 2003, 582, 984
- Pereyra, N. A., Owocki, S. P., Hillier, D. J., & Turnshek, D. A. 2004, *ApJ*, 608, 454 (Paper I)
- Pereyra, N. A. 2005, *ApJ*, 622, 577 (Paper II)
- Shakura, N. I., & Sunyaev, R. A. 1973, *A&A*, 24, 337
- Turnshek, D. A. 1984, *ApJ*, 278, L87
- Warner, B. 1995, *Cataclysmic Variable Stars*, (Cambridge University Press)

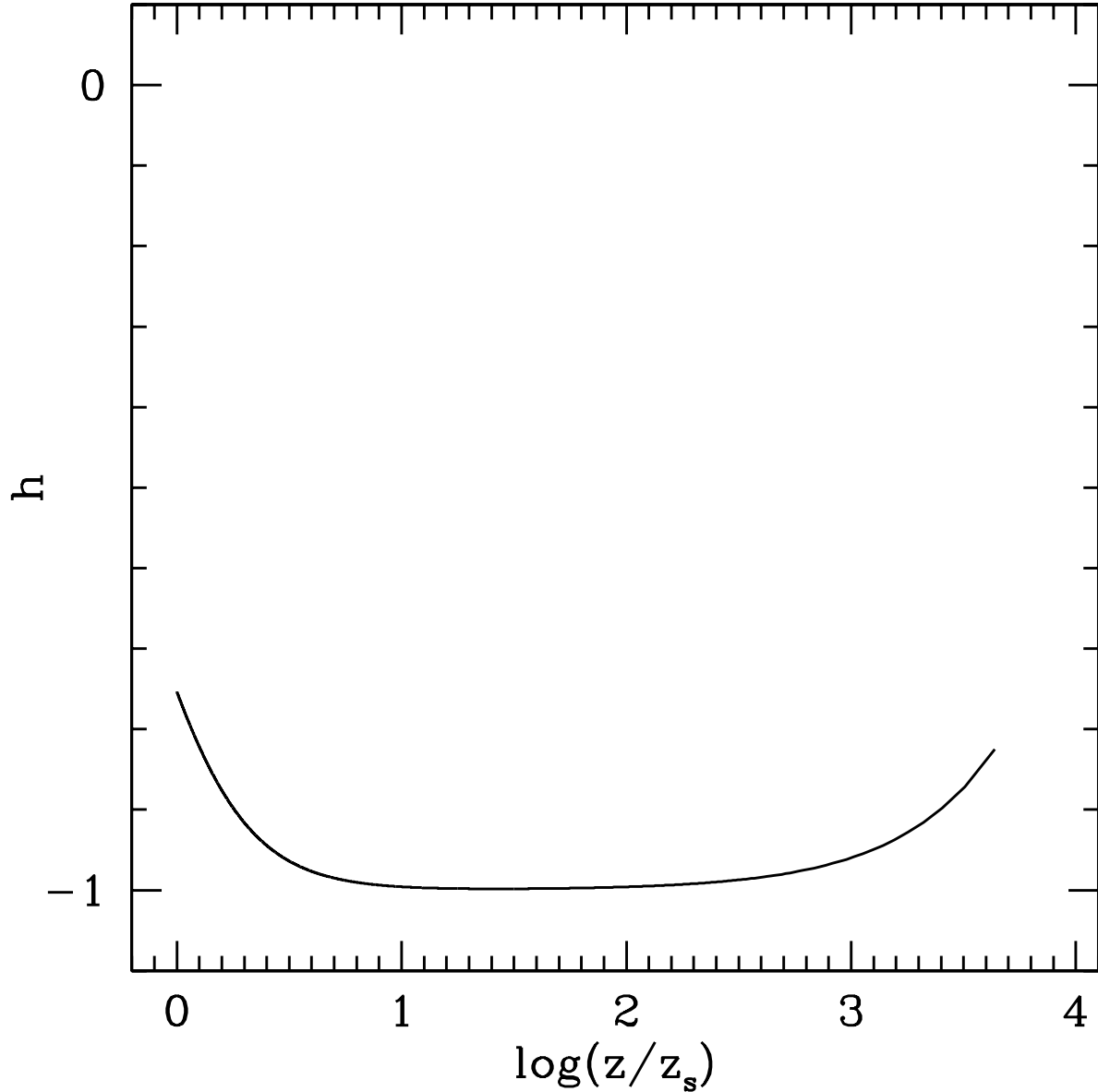


Fig. 1.— The h function for the 1D vertical wind model with the flux distribution of a standard Shakura-Sunyaev disk at $r = 2r_i$. A necessary requirement for the critical point is that the h function must be negative at that point. This figure shows that all points ranging from the sonic point to beyond 1000 times the sonic height fulfill this condition. The physical parameters used are: $M = 0.6 M_\odot$, $\mathcal{L}_{disk} = \mathcal{L}_\odot$, $z_s = 0.0229 R_\odot$, $r_i = 0.01 R_\odot$, $b = 10 \text{ km s}^{-1}$, $V_{th} = 2.67 \text{ km s}^{-1}$, $k = 1/3$, and $\alpha = 0.7$.

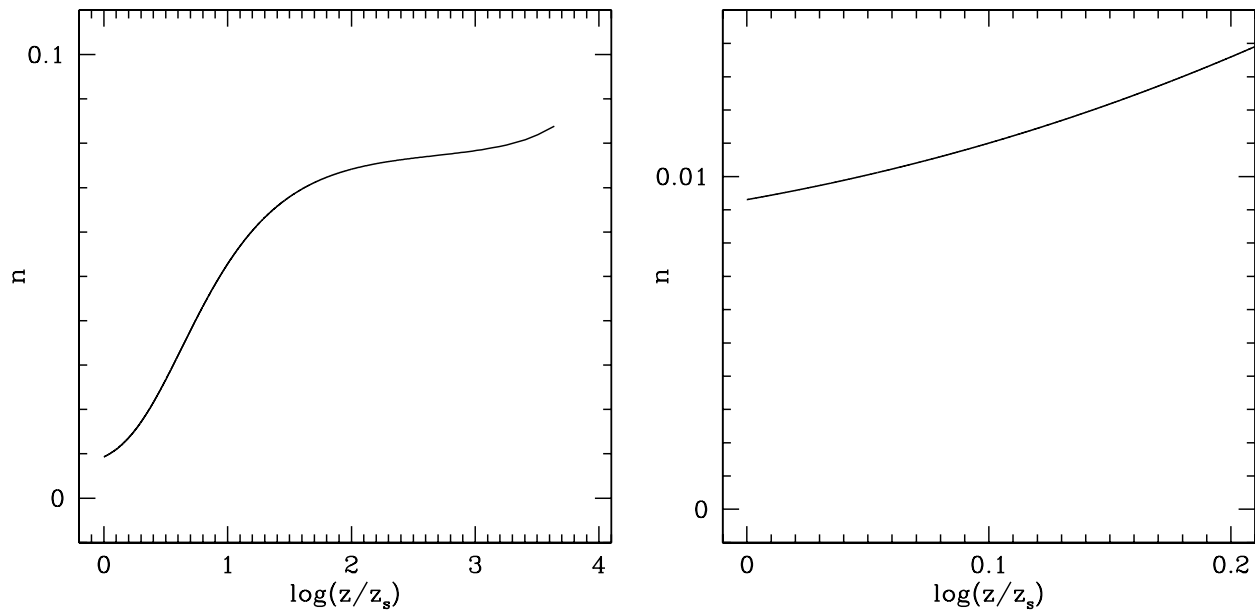


Fig. 2.— The nozzle function n for the 1D vertical wind model with the flux distribution of a standard Shakura-Sunyaev disk at $r = 2r_i$. A necessary requirement for the critical point in an isothermal line-driven wind is that the nozzle function must be locally increasing (i.e., $dn/dq > 0$ [$dn/dz > 0$]) at that point. This figure shows that all points ranging from the sonic point to beyond 1000 times the sonic height fulfill this condition. The physical parameters used are the same as in Figure 1.

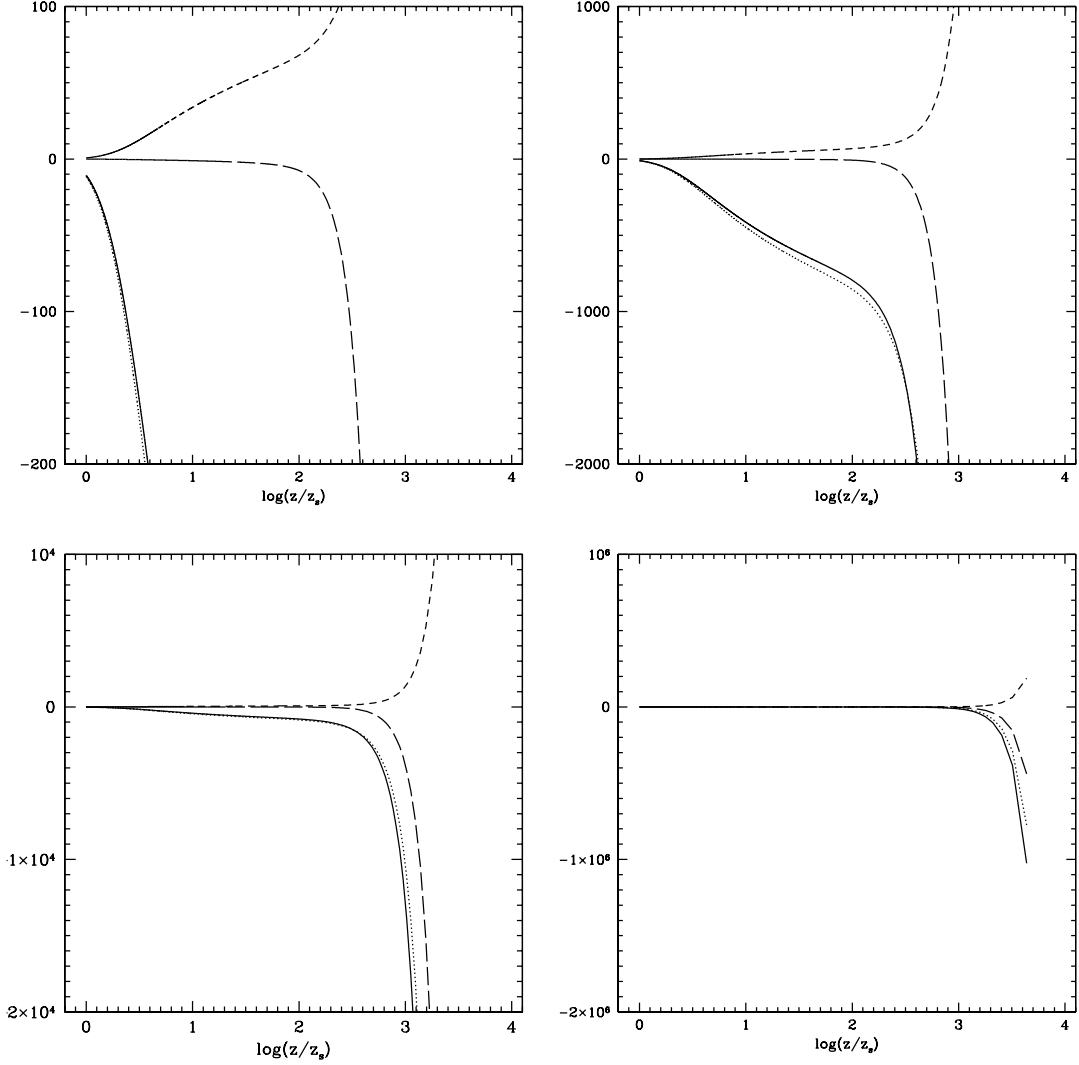


Fig. 3.— Local solution existence for the 1D vertical wind model with the flux distribution of a standard Shakura-Sunyaev disk at $r = 2r_i$: a local solution exists in the vicinity of a critical point z if the expression $\beta'' \dot{m} (\omega')^2 + \beta' \dot{m} \omega'' - n''$ (solid curve) is negative. This figure shows that all points ranging from the sonic point to beyond 1000 times the sonic height fulfill this condition. In this plot the terms $\beta'' \dot{m} (\omega')^2$ (dotted curve), $\beta' \dot{m} \omega''$ (short dash curve), and $-n''$ (long dash curve) are also shown. The physical parameters used are the same as in Figure 1.

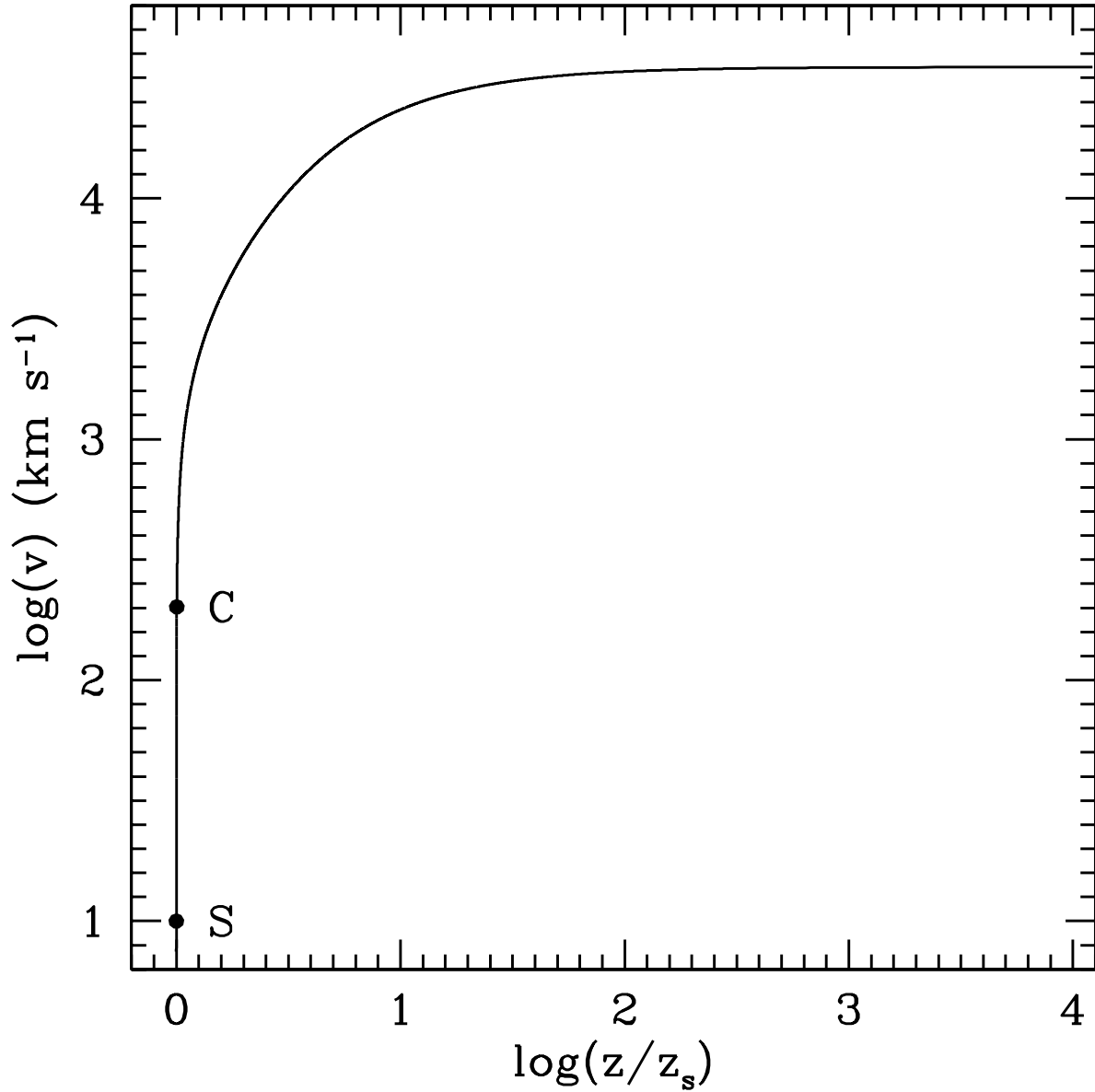


Fig. 4.— Velocity vs. position for the 1D vertical wind model with the flux distribution of a standard Shakura-Sunyaev disk at $r = 2r_i$. The critical point position is determined with the condition that, upon integration of the equation of motion, the correct sonic point position is found. “C” indicates the critical point and “S” indicates the sonic point. The physical parameters used are the same as in Figure 1.

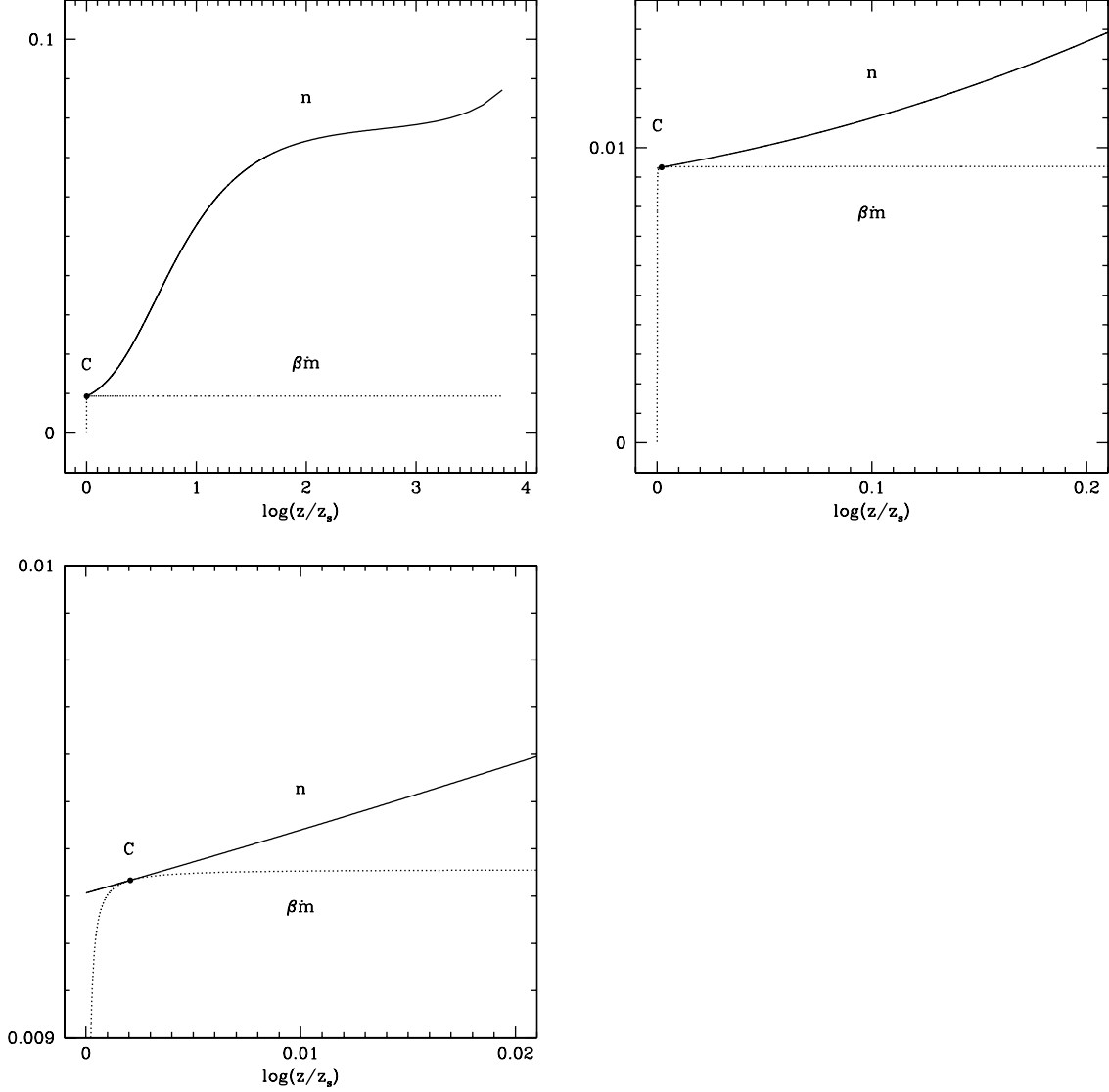


Fig. 5.— Necessary condition for the global solution existence for the 1D vertical wind model with flux distribution of a standard Shakura-Sunyaev disk at $r = 2r_i$ for the critical point shown in Figure 4: upon the integration of the equation of motion, it must hold that $\beta(\omega) \dot{m} < n(q)$ at points other than the critical point [when $h(q) < 0$ and the wind is supersonic], and $\beta(\omega) \dot{m} = n(q)$ at the critical point. Presented here is the nozzle function n (solid curve) and the $\beta \dot{m}$ function (dotted curve) vs. position. “C” indicates the critical point. The physical parameters used are the same as in Figure 1.

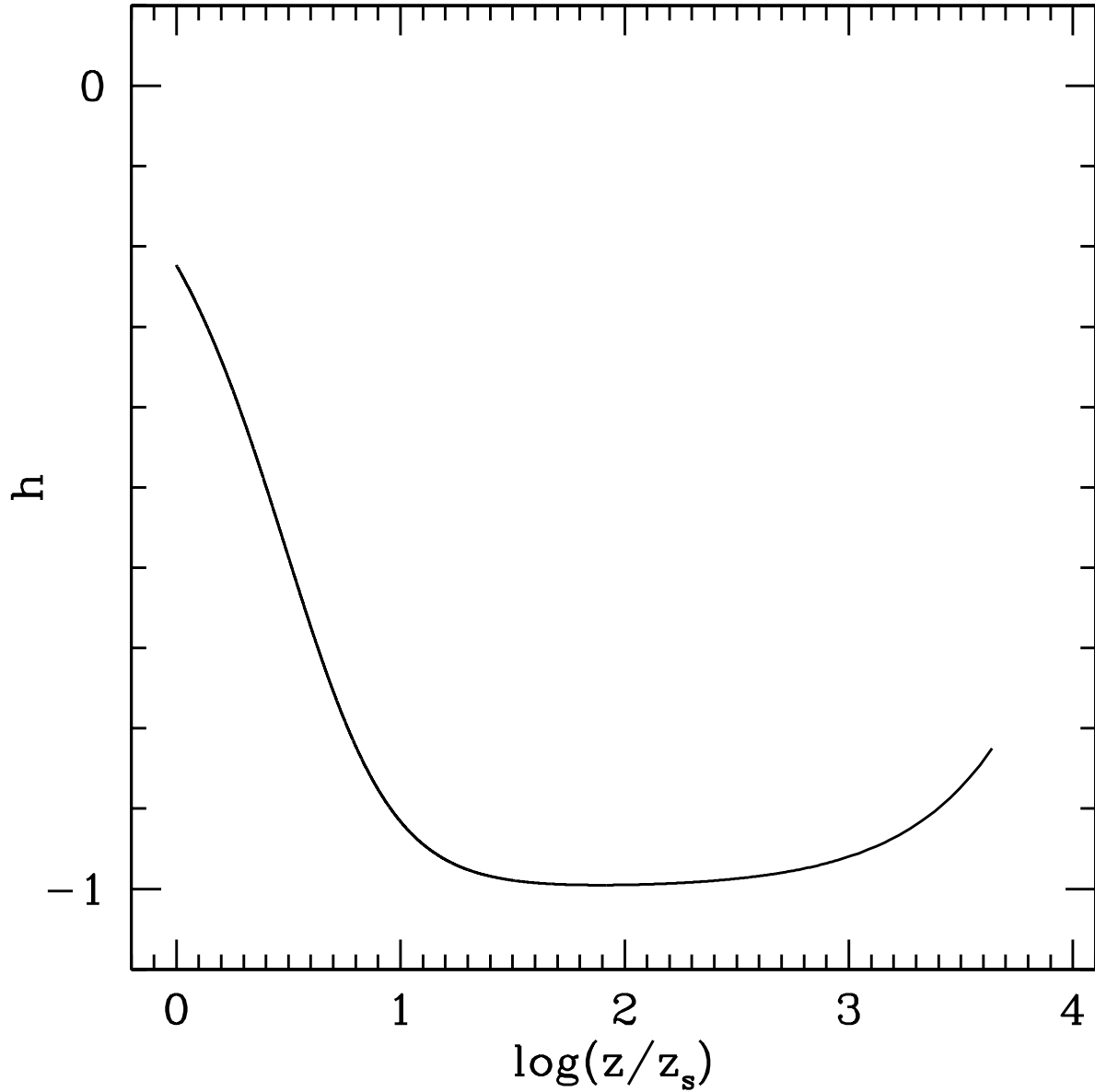


Fig. 6.— The h function for the 1D vertical wind model with the flux distribution of a standard Shakura-Sunyaev disk at $r = 10 r_i$. A necessary requirement for the critical point is that the h function must be negative at that point. This figure shows that all points ranging from the sonic point to beyond 1000 times the sonic height fulfill this condition. The physical parameters used are the same as in Figure 1.

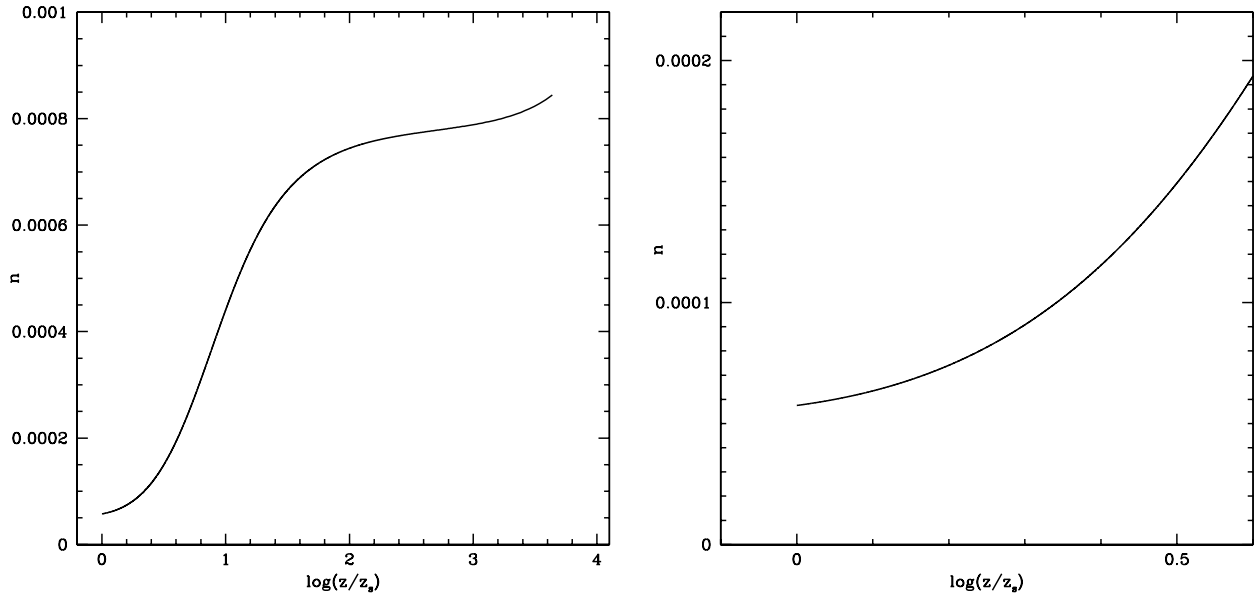


Fig. 7.— The nozzle function n for the 1D vertical wind model with the flux distribution of a standard Shakura-Sunyaev disk at $r = 10 r_i$. A necessary requirement for the critical point in an isothermal line-driven wind is that the nozzle function must be locally increasing (i.e., $dn/dq > 0$) at that point. This figure shows that all points ranging from the sonic point to beyond 1000 times the sonic height fulfill this condition. The physical parameters used are the same as in Figure 1.

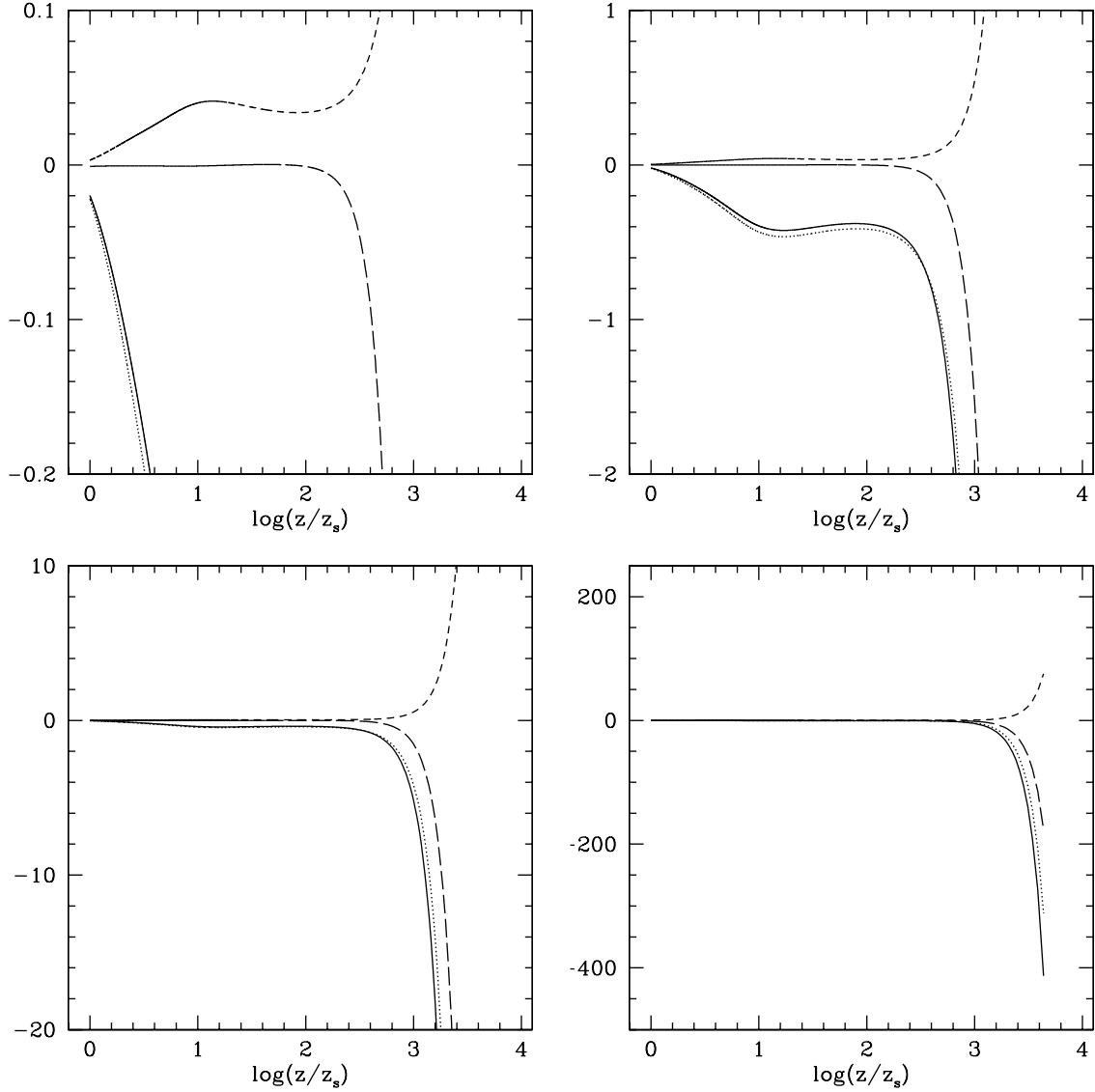


Fig. 8.— Local solution existence for the 1D vertical wind model with the flux distribution of a standard Shakura-Sunyaev disk at $r = 10 r_i$: a local solution exists in the vicinity of a critical point z if the expression $\beta'' \dot{m} (\omega')^2 + \beta' \dot{m} \omega'' - n''$ (solid curve) is negative. This figure shows that all points ranging from the sonic point to beyond 1000 times the sonic height fulfill this condition. In this plot the terms $\beta'' \dot{m} (\omega')^2$ (dotted curve), $\beta' \dot{m} \omega''$ (short dash curve), and $-n''$ (long dash curve) are also shown. The physical parameters used are the same as in Figure 1.

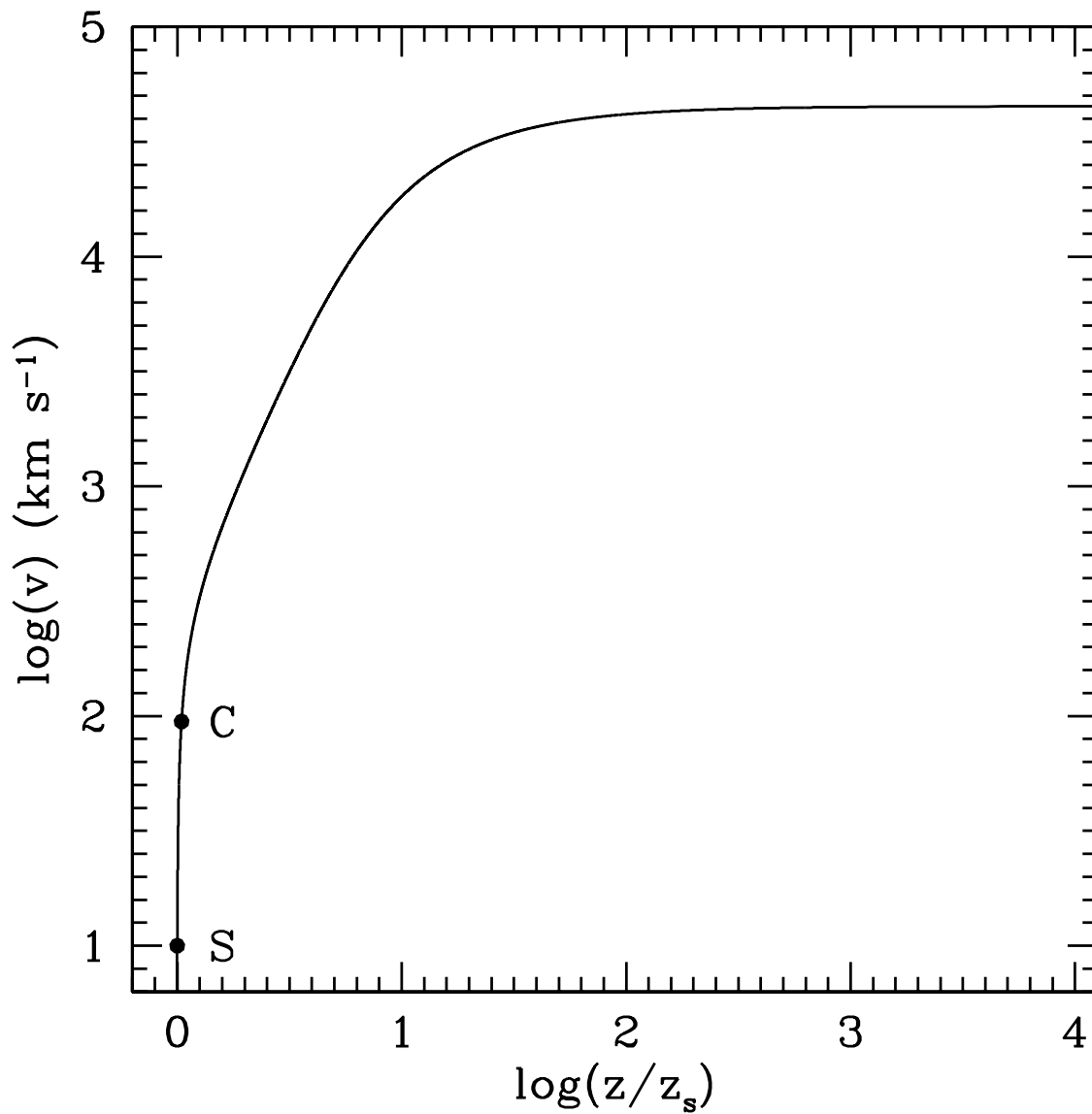


Fig. 9.— Velocity vs. position for the 1D vertical wind model with the flux distribution of a standard Shakura-Sunyaev disk at $r = 10 r_i$. The critical point position is determined with the condition that, upon integration of the equation of motion, the correct sonic point position is found. “C” indicates the critical point and “S” indicates the sonic point. The physical parameters used are the same as in Figure 1.

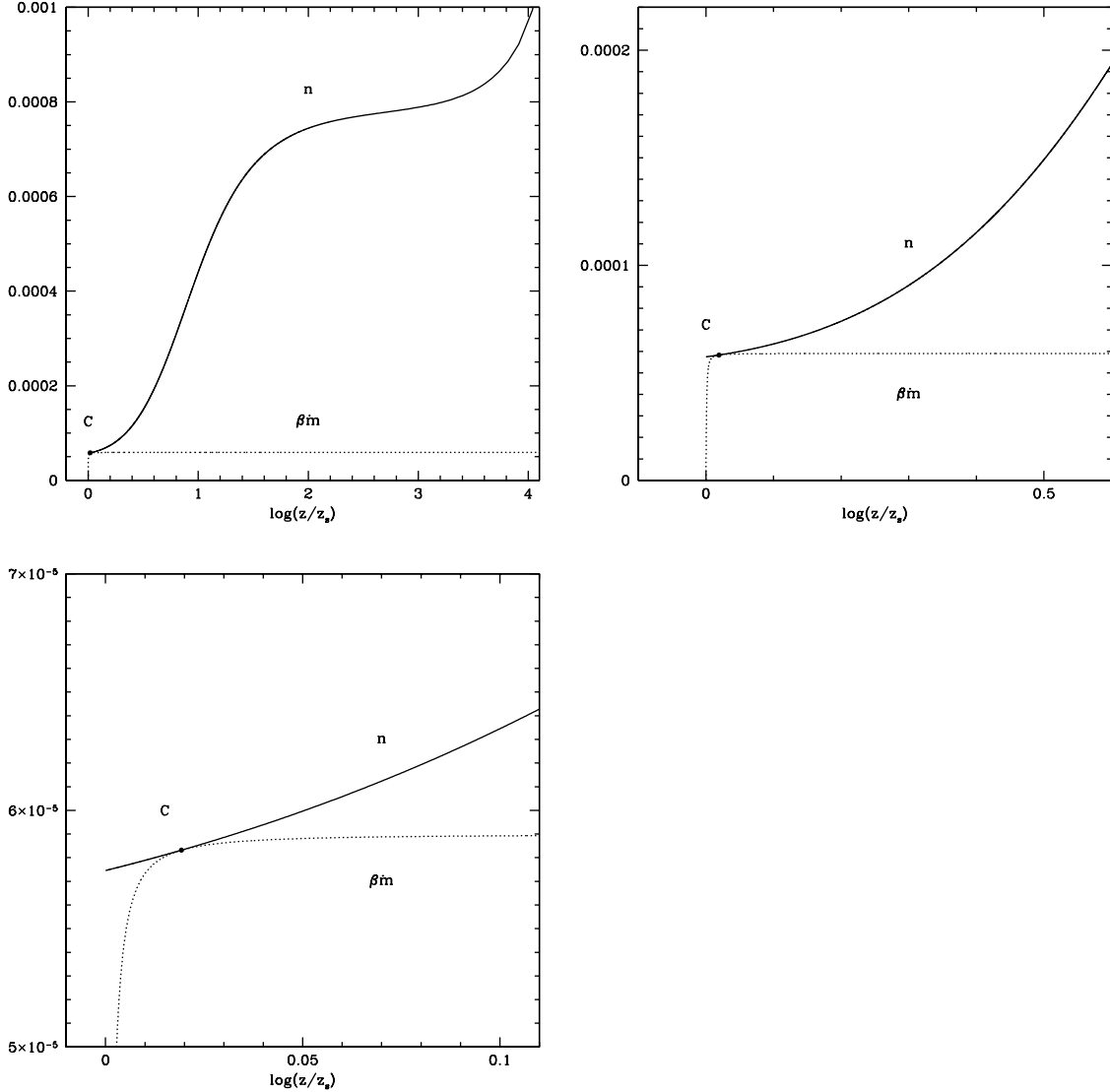


Fig. 10.— Necessary condition for the global solution existence for the 1D vertical wind model with the flux distribution of a standard Shakura-Sunyaev disk at $r = 10 r_i$ for the critical point shown in Figure 9: upon the integration of the equation of motion, it must hold that $\beta(\omega) \dot{m} < n(q)$ at points other than the critical point [when $h(q) < 0$ and the wind is supersonic], and $\beta(\omega) \dot{m} = n(q)$ at the critical point. Presented here is the nozzle function n (solid curve) and the $\beta \dot{m}$ function (dotted curve) vs. position. “C” indicates the critical point. The physical parameters used are the same as in Figure 1.

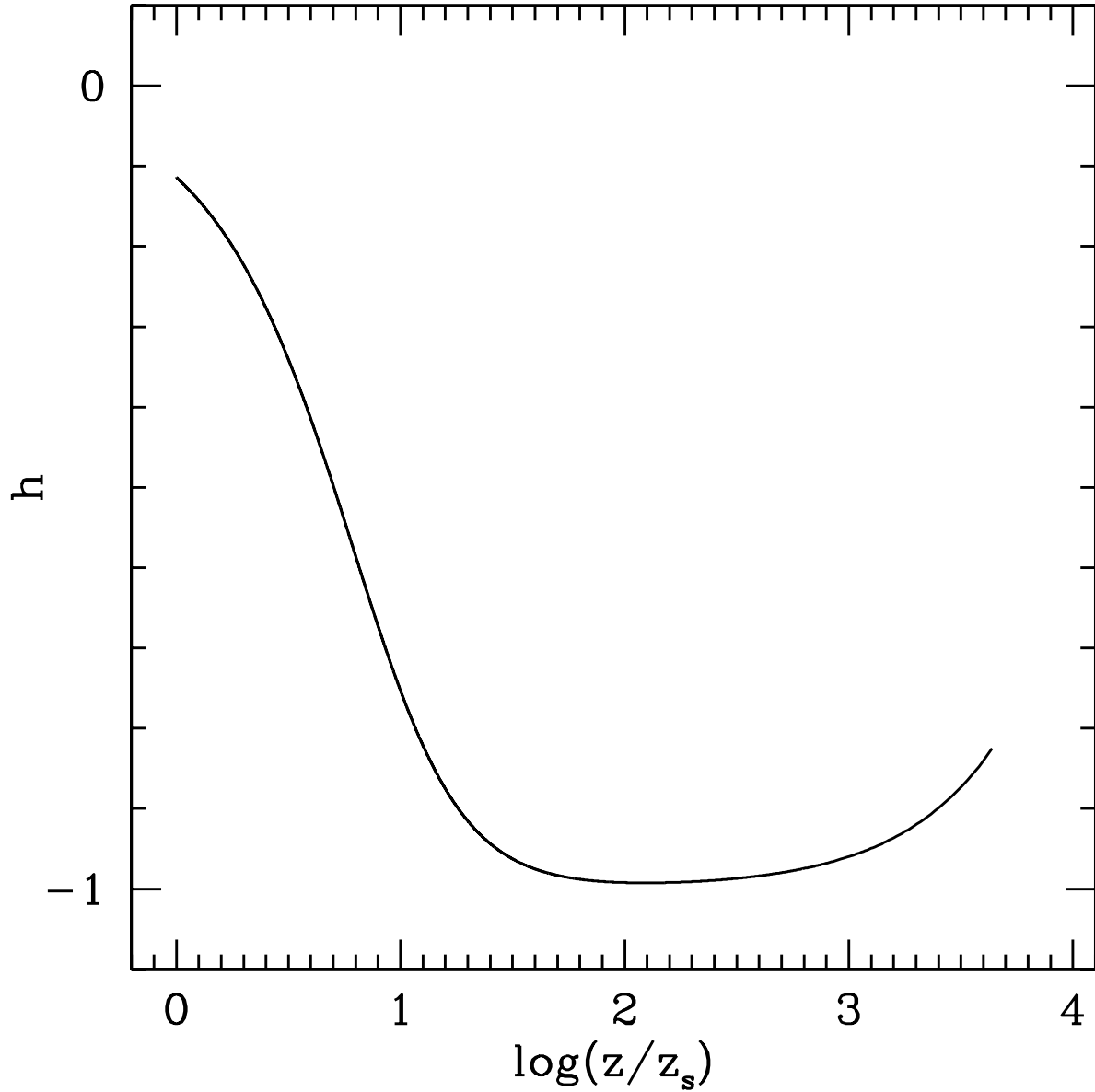


Fig. 11.— The h function for the 1D vertical wind model with the flux distribution of a standard Shakura-Sunyaev disk at $r = 20 r_i$. A necessary requirement for the critical point is that the h function must be negative at that point. This figure shows that all points ranging from the sonic point to beyond 1000 times the sonic height fulfill this condition. The physical parameters used are the same as in Figure 1.

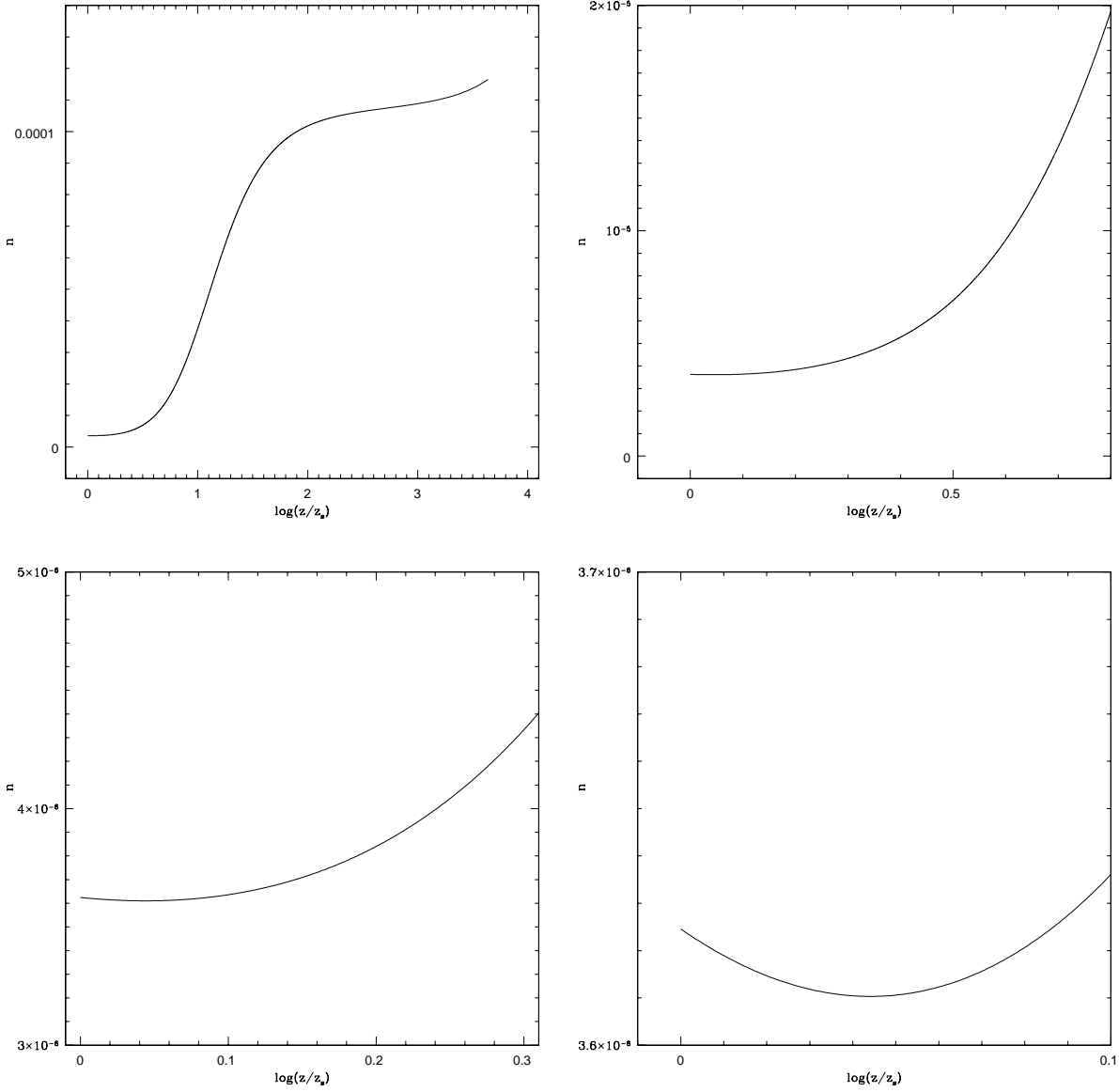


Fig. 12.— The nozzle function n for the 1D vertical wind model with the flux distribution of a standard Shakura-Sunyaev disk at $r = 20 r_i$. A necessary requirement for the critical point in an isothermal line-driven wind is that the nozzle function must be locally increasing (i.e., $dn/dq > 0$) at that point. This figure shows that all points ranging from ≈ 1.107 times the sonic height to beyond 1000 times the sonic height fulfill this condition. However, it is also shown that points ranging from the sonic point up to ≈ 1.107 times the sonic height do not fulfill the condition. The physical parameters used are the same as in Figure 1.

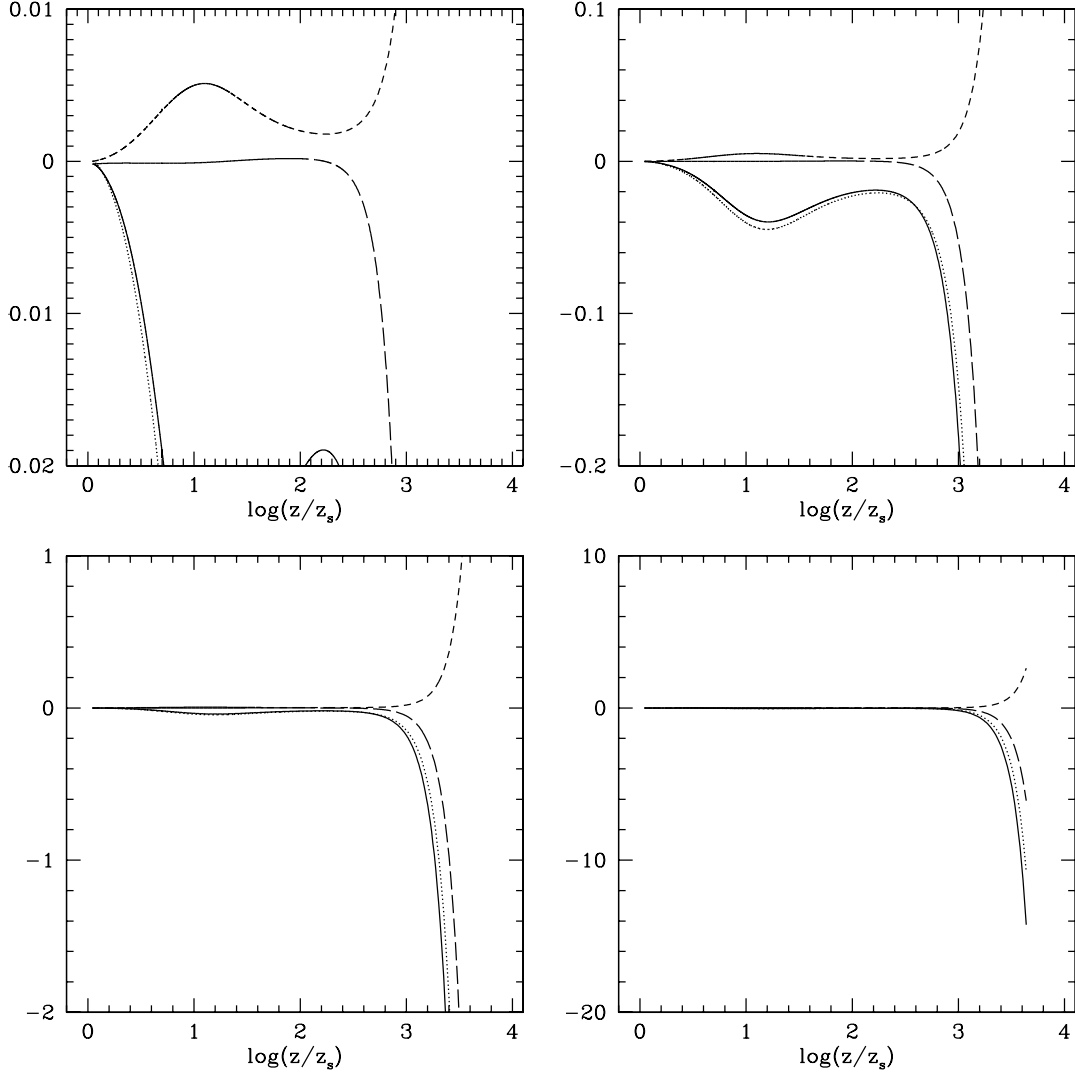


Fig. 13.— Local solution existence for the 1D vertical wind model with the flux distribution of a standard Shakura-Sunyaev disk at $r = 20 r_i$: a local solution exists in the vicinity of a critical point z if the expression $\beta'' \dot{m} (\omega')^2 + \beta' \dot{m} \omega'' - n''$ (solid curve) is negative. This figure shows that all points ranging from ≈ 1.107 times the sonic height to beyond 1000 times the sonic height fulfill this condition. From ≈ 1.107 times the sonic height down to the sonic point, the critical point conditions cannot be met (see Figure 12). In this plot the terms $\beta'' \dot{m} (\omega')^2$ (dotted curve), $\beta' \dot{m} \omega''$ (short dash curve), and $-n''$ (long dash curve) are also shown. The physical parameters used are the same as in Figure 1.

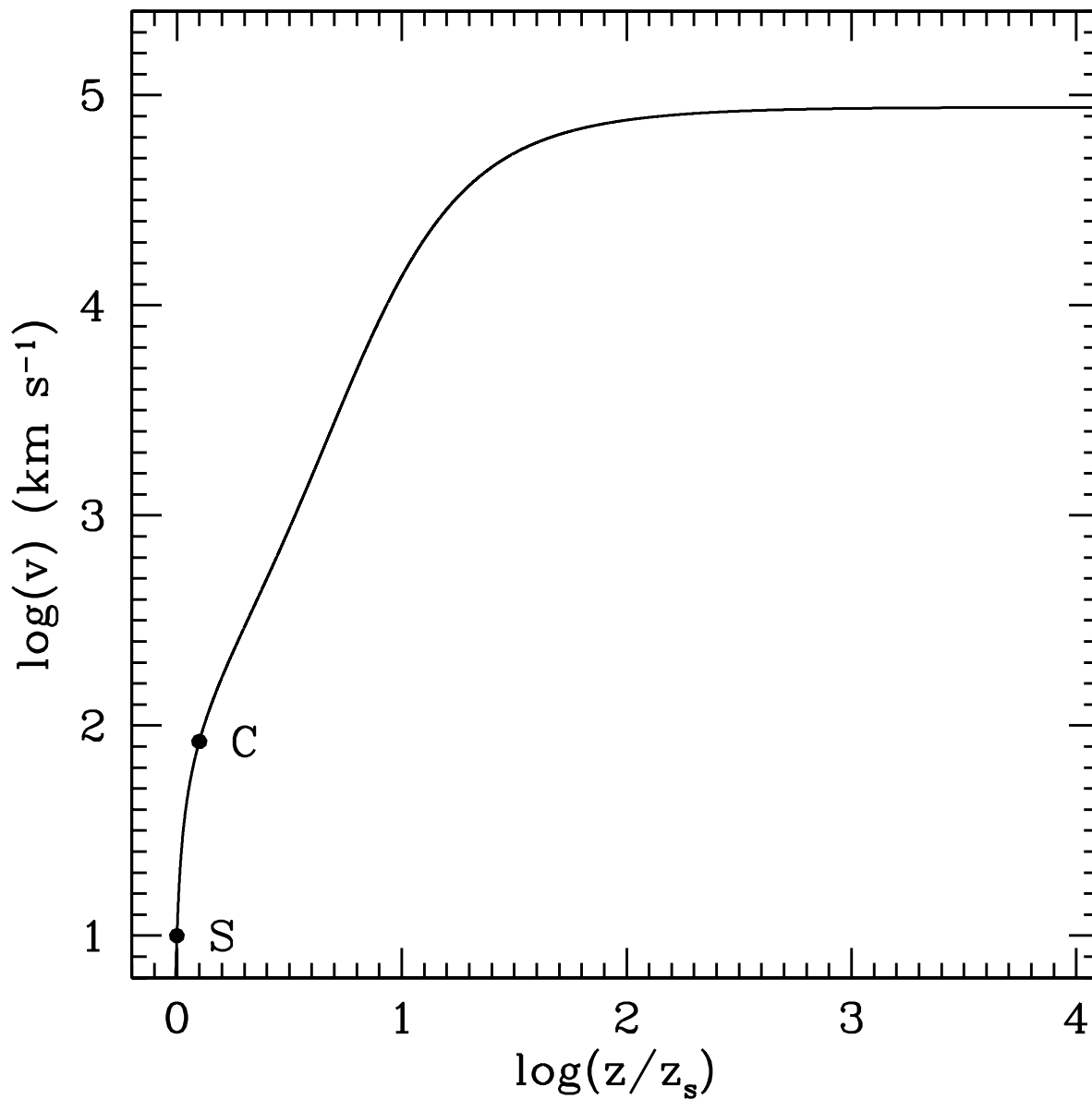


Fig. 14.— Velocity vs. position for the 1D vertical wind model with the flux distribution of a standard Shakura-Sunyaev disk at $r = 20 r_i$. The critical point position is determined with the condition that, upon integration of the equation of motion, the correct sonic point position is found. “C” indicates the critical point and “S” indicates the sonic point. The physical parameters used are the same as in Figure 1.

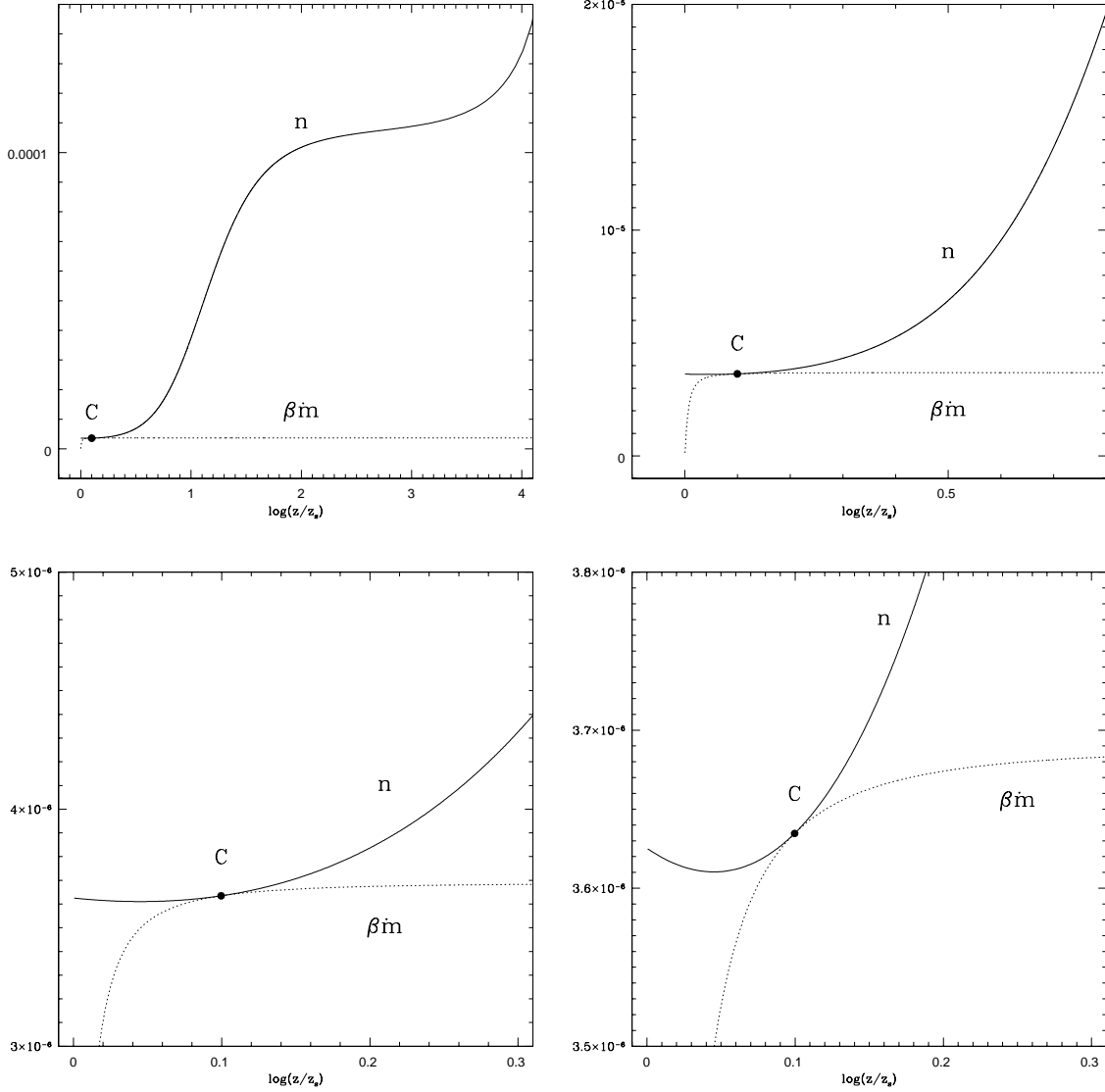


Fig. 15.— Necessary condition for the global solution existence for the 1D vertical wind model with the flux distribution of a standard Shakura-Sunyaev disk at $r = 20 r_i$ for the critical point shown in Figure 14: upon the integration of the equation of motion, it must hold that $\beta(\omega) \dot{m} < n(q)$ at points other than the critical point [when $h(q) < 0$ and the wind is supersonic], and $\beta(\omega) \dot{m} = n(q)$ at the critical point. Presented here is the nozzle function n (solid curve) and the $\beta \dot{m}$ function (dotted curve) vs. position. “C” indicates the critical point. The physical parameters used are the same as in Figure 1.

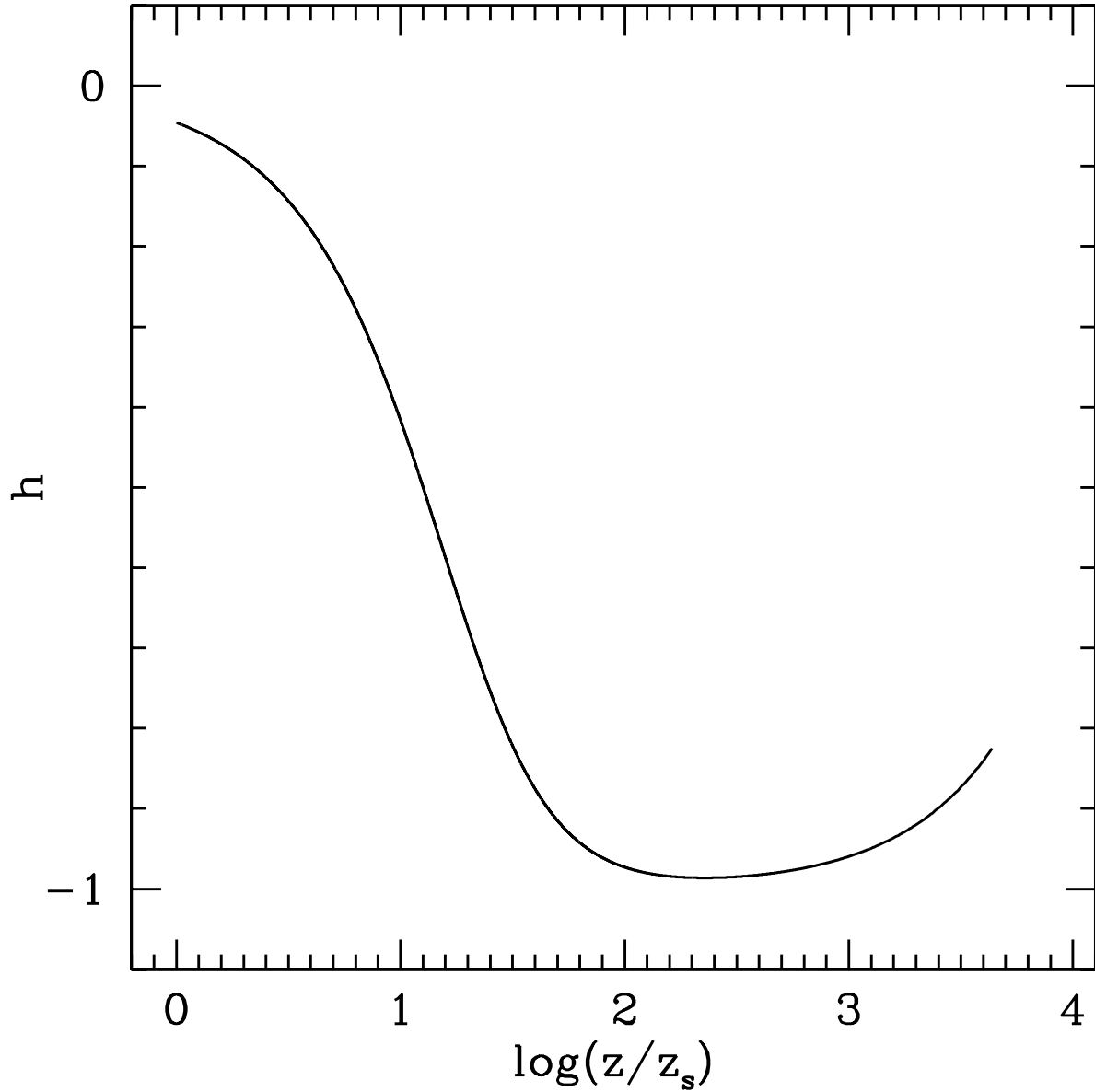


Fig. 16.— The h function for the 1D vertical wind model with the flux distribution of a standard Shakura-Sunyaev disk at $r = 50 r_i$. A necessary requirement for the critical point is that the h function must be negative at that point. This figure shows that all points ranging from the sonic point to beyond 1000 times the sonic height fulfill this condition. The physical parameters used are the same as in Figure 1.

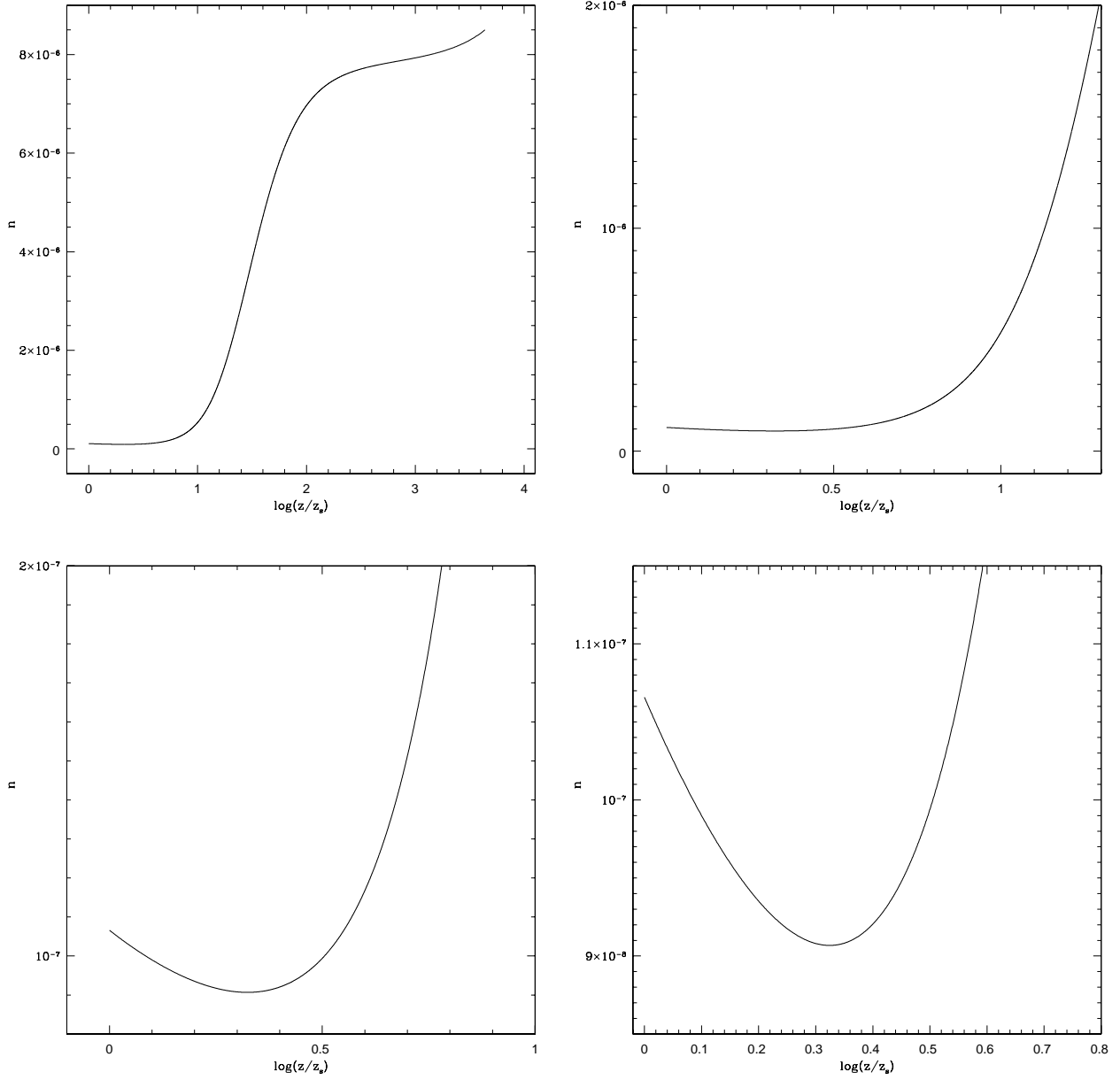


Fig. 17.— The nozzle function n for the 1D vertical wind model with the flux distribution of a standard Shakura-Sunyaev disk at $r = 50 r_i$. A necessary requirement for the critical point in an isothermal line-driven wind is that the nozzle function must be locally increasing (i.e., $dn/dq > 0$) at that point. This figure shows that all points ranging from ≈ 2.11 times the sonic height to beyond 1000 times the sonic height fulfill this condition. However, it is also shown that points ranging from the sonic point up to ≈ 2.11 times the sonic height do not fulfill the condition. The physical parameters used are the same as in Figure 1.

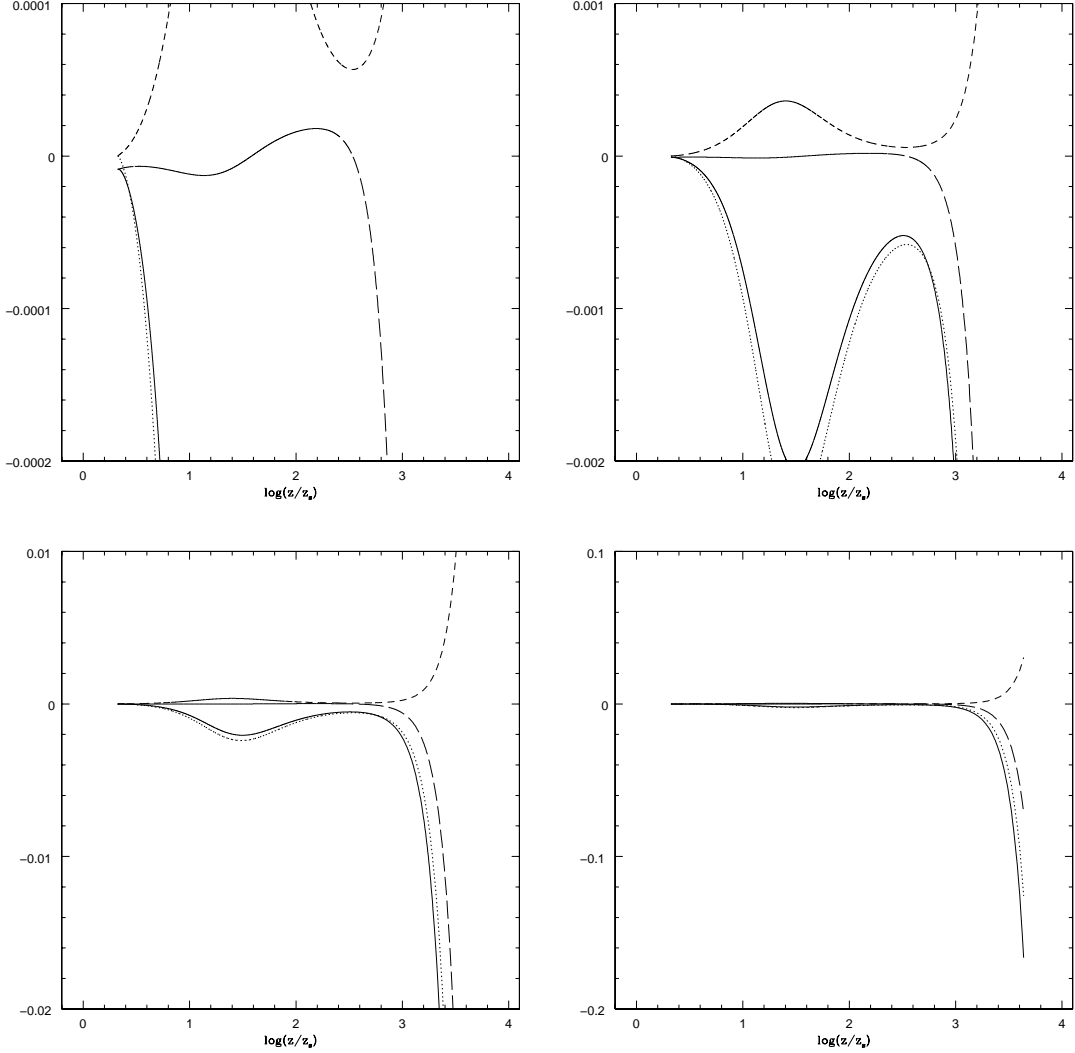


Fig. 18.— Local solution existence for the 1D vertical wind model with the flux distribution of a standard Shakura-Sunyaev disk at $r = 50 r_i$: a local solution exists in the vicinity of a critical point z if the expression $\beta'' \dot{m} (\omega')^2 + \beta' \dot{m} \omega'' - n''$ (solid curve) is negative. This figure shows that all points ranging from ≈ 2.11 times the sonic height to beyond 1000 times the sonic height fulfill this condition. From ≈ 2.11 times the sonic height down to the sonic point, the critical point conditions cannot be met (see Figure 17). In this plot the terms $\beta'' \dot{m} (\omega')^2$ (dotted curve), $\beta' \dot{m} \omega''$ (short dash curve), and $-n''$ (long dash curve) are also shown. The physical parameters used are the same as in Figure 1.

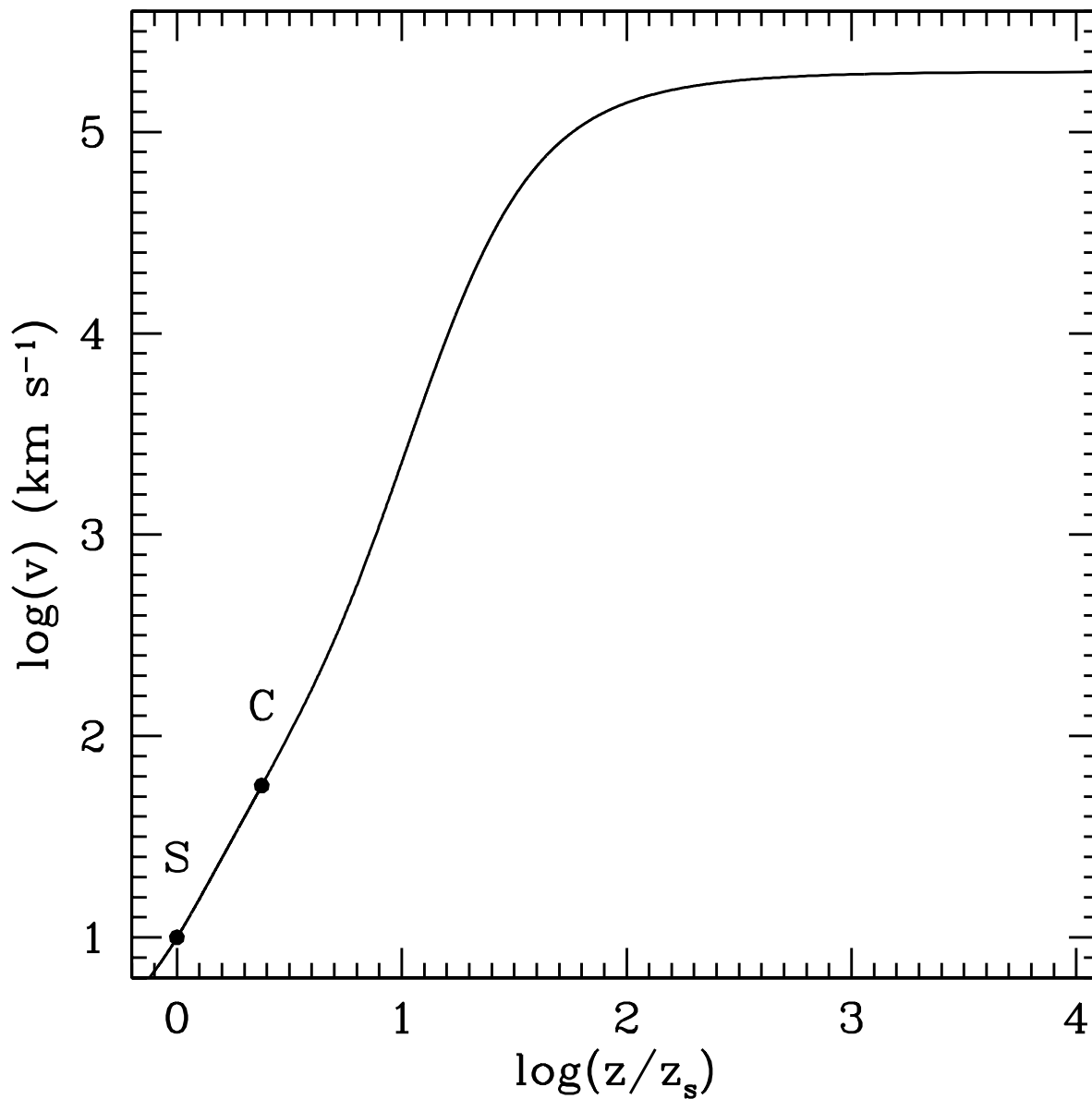


Fig. 19.— Velocity vs. position for the 1D vertical wind model with the flux distribution of a standard Shakura-Sunyaev disk at $r = 50 r_i$. The critical point position is determined with the condition that, upon integration of the equation of motion, the correct sonic point position is found. “C” indicates the critical point and “S” indicates the sonic point. The physical parameters used are the same as in Figure 1.

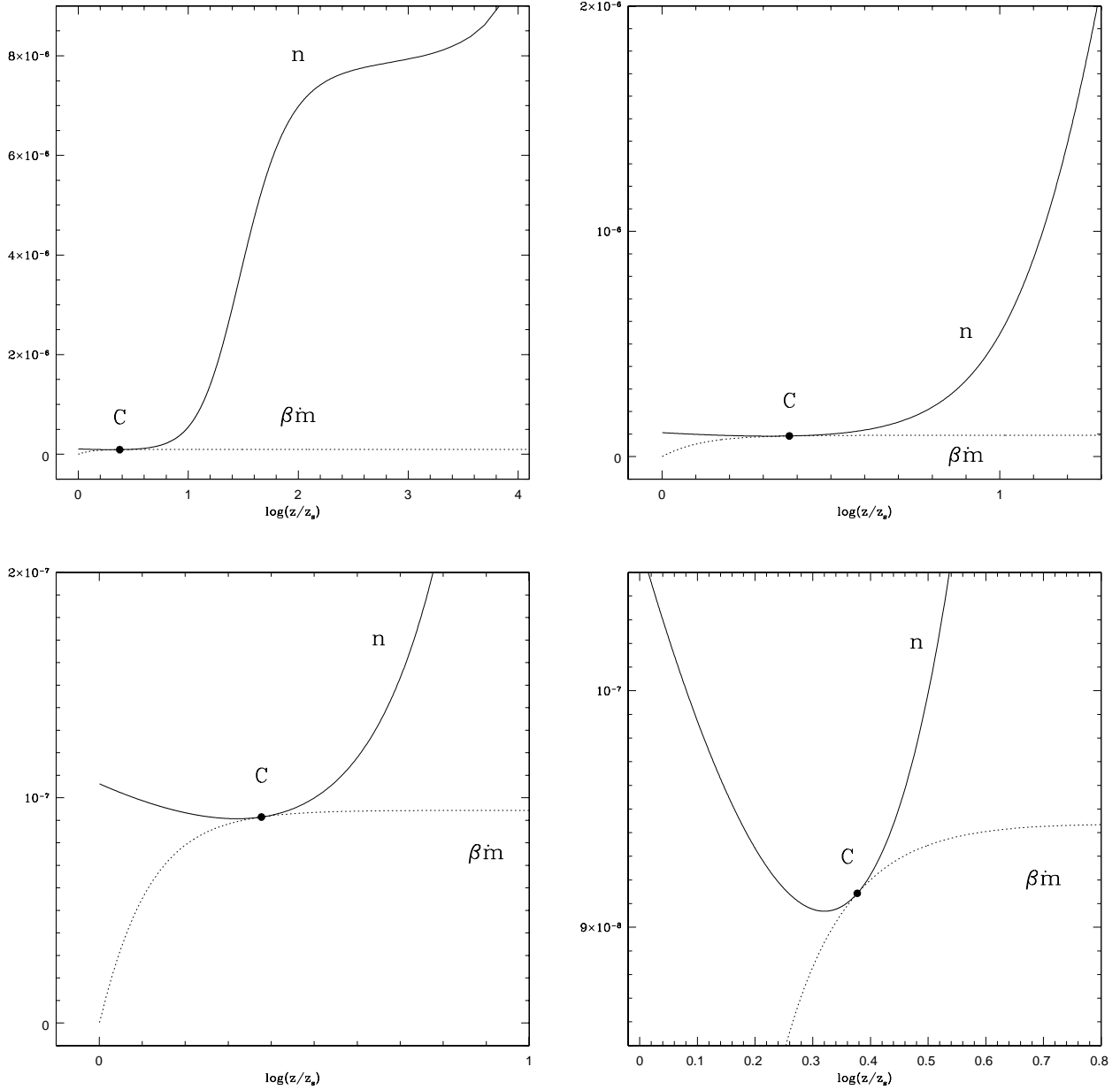


Fig. 20.— Necessary condition for the global solution existence for the 1D vertical wind model with the flux distribution of a standard Shakura-Sunyaev disk at $r = 50 r_i$ for the critical point shown in Figure 19: upon the integration of the equation of motion, it must hold that $\beta(\omega) \dot{m} < n(q)$ at points other than the critical point [when $h(q) < 0$ and the wind is supersonic], and $\beta(\omega) \dot{m} = n(q)$ at the critical point. Presented here is the nozzle function n (solid curve) and the $\beta \dot{m}$ function (dotted curve) vs. position. “C” indicates the critical point. The physical parameters used are the same as in Figure 1.